Energy 330 (2025) 136843

Contents lists available at ScienceDirect

Energy

journal homepage: www.elsevier.com/locate/energy

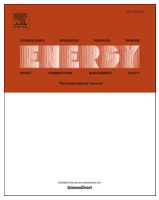

A techno-economic analysis of a high vacuum solar system integrated into a prosumer-based district heating network

Giuseppe Edoardo Dino *, Pietro Catrini, Maurizio La Villetta, Antonio Piacentino

Department of Engineering, University of Palermo, Palermo, Italy

ARTICLE INFO

Handling Editor: Neven Duic

Keywords:
Bidirectional thermal district
Distributed generation
Active district heating
Bidirectional substation
Prosumer
Solar energy
Thermal curtailment

ABSTRACT

Sharing thermal energy from distributed solar plants through district heating networks is recognized to be crucial in the transition to 100 % renewable systems. However, few studies have explored the benefits and challenges for users who install solar thermal plants and sell surplus heat to the network, thus becoming "prosumers". Through a validated model of a bidirectional district heating substation, this paper examines the feasibility of integrating high vacuum solar thermal technology into an office building connected to a district heating network in Mediterranean regions. The heat generated by solar collectors is utilized not only during the heating season but also in the cooling period through an absorption chiller, with the possibility of delivering the heat surplus to a thermal network. The study investigates different scenarios based on different sizes of the solar system to analyze the impact on energy savings and profitability. Results show that being a prosumer highly increases the exploitation of the heat produced by the solar plant and lets it cover up to 73.8 % of the heating demand by solar energy and up to 43 % of the cooling demand by the absorption chiller. The economic analysis indicates that incorporating an absorption chiller may render the investment unprofitable, highlighting the need for a targeted financial support system. Moreover, the importance of minimizing thermal energy curtailment is evidenced. The present work provides a preliminary assessment of the potential benefits and challenges arising for a thermal prosumer with high-vacuum collectors in Mediterranean regions with moderate climatic conditions while pointing out the future routes to be investigated for promoting the spread of small-scale solar prosumers in district heating and cooling networks.

1. Introduction

In 2022, the household sector of the European Union (EU) accounted for 26.9 % (1411 TWh) of final energy consumption [1]. Specifically, space heating represents the primary use of energy in households, accounting for 63.5 %. A significant portion of this demand was still met by fossil fuels, although renewable energy sources (RES) contributed over a quarter of the total, reaching 31.4 % [2]. Water heating represents the second largest share, whereas space cooling plays only a minor role.

Improving energy efficiency in buildings is one of the pillars in the EU plan "Fit for 55 %" [3]. In this framework, the district heating and cooling networks (DHCN) can make a relevant and fast contribution to the decarbonization of this sector. However, this potential remains largely untapped as many countries have opportunities to develop new DHCNs, improve the energy efficiency of aging systems (such as by upgrading insulation and substituting heat generators), and integrate RES into existing networks. [4]. In this respect, in the framework of the RewardHeat project [5], the TIMES (The Integrated MARKAL-EFOM System) model was developed to provide a quantification of the potential of DHCNs in a given region [6].

Great interest in the research has been paid for lowering the district heating operating temperature to integrate thermal energy from RES (such as solar plants) or heat pumps and to reduce the heat losses in the pipelines. In this respect, the concept of fourth-generation district heating networks (4GDHN) was introduced, characterized by operating temperatures below 60 °C [7]. These new thermal grids allow for the sharing of RES across the entire districts, and the network could act as heat storage as well [8]. For instance, in Ref. [9], a novel low-temperature DH system composed of an absorption heat pump that uses low-temperature heat extracted by a geothermal plant and steam from a waste incineration plant was presented. The application of the proposed system to Frederikshavn (DK) reported a primary energy

This article is part of a special issue entitled: SDEWES 2024 published in Energy.

* Corresponding author.
E-mail address: giuseppeedoardo.dino@unipa.it (G.E. Dino).

https://doi.org/10.1016/j.energy.2025.136843
Received 3 December 2024; Received in revised form 24 May 2025; Accepted 25 May 2025
Available online 26 May 2025

savings of up to 26 %. Another study [10] proposed the adoption of multiple technologies for DHC to enhance the exploitation of waste heat. In Ref. [11], the authors investigated the integration of waste heat into the DHN at Forschungszentrum Jülich (FZJ), Germany. A Modelica simulation was extended to assess waste heat from a new HPC facility. Lowering supply temperatures from 95–132 °C to 80–100 °C reduces heat losses and improves heat pump efficiency. Results show that up to 40 % waste heat integration is feasible without compromising network operations, with a 65 °C return temperature critical for CHP constraints. However, a significant challenge with 4GDHN is still related to the intensive exploitation of waste heat at a very low temperature (lower than 50 °C). This limitation has led to the development of the Fifth Generation District Heating and Cooling (5GDHN) [12]. Here, 5GDHNs are characterized by operating at temperatures close to the ground levels, enabling the integration of decentralized heat producers and the bidirectional heat exchange [13]. Specifically, they could be coupled with decentralized heat pumps thus allowing for a full integration of the electric power grid and DHCNs [14].

DHCNs are also included in energy-sharing models. In this context, "Integrated Energy Communities" present new opportunities to develop smarter, more flexible, and interconnected local systems with positive effects on environmental, economic, and social sustainability [15]. While "Electrical Energy Communities" have already established a recognized and structured framework, "Thermal Energy Communities" still require further research to overcome barriers that hinder their feasibility [16]. Among these, it is worth mentioning the impact on the thermohydraulic behavior of the DHN resulting from the increasing number of RES producers capable of supplying heat to thermal grids [17]. Notably, a typical heat consumer connected to the network may become a producer for several hours a day, thanks to energy generated by onsite RES systems [18]. As in the case of the electricity grid, such an actor is not more classified as a “consumer”, but it is a “prosumer” (i.e., “producer-consumer”) [19]. From a technological perspective, in Ref. [20], an experimental layout for a prosumer’s thermal substation was proposed and tested under different conditions. The authors claimed that the proposed return-to-supply configuration is the most reliable one for bidirectional heat exchange within DHNs. The same system was then adopted for another research [21], where a hardware-in-the-loop methodology showed significant variations in local energy contributions, achieving up to 100 % from waste heat. The experimental test presented in Ref. [22] investigates the integration of heat prosumers in thermal networks through bi-directional heat trading. The experimental study demonstrates operational feasibility, achieving a temperature range of 11 °C–13 °C and potential carbon emission reductions of 12.7 %.

The presence of thermal prosumers also necessitates novel simulation tools to model, simulate, and optimize the performance and economic viability of DHN, focusing on dynamic behavior and economic analysis. A mathematical model for decentralized thermal networks dominated by prosumers was introduced in Ref. [23], integrating hydraulic and thermal dynamics. It highlighted the sensitivity of system performance to control variables and emphasized the importance of smart control strategies.

The experimental study presented in Ref. [24] examined the challenges faced by experimental facilities to test a DHC system. A Power Hardware In the Loop experimental facility replicated a network architecture composed of five thermal and electric prosumer houses that are connected with a thermal and electric grid. The examined case studies revealed that prosumer integration into flexible DHC grids can lower heating costs. However, it was found that simplistic control strategies may not suffice when multiple prosumers are feeding into the system. An application of the virtual model of a validated prosumer substation was obtained in the TRNSYS environment [25], which was then implemented to obtain a heuristic profit-oriented management strategy of a heat pump connected in prosumer operation mode [26].

In [27], the authors investigated the use of solar thermal energy in prosumer substations while proposing a retrofit for bidirectional heat exchange. It was found that although DHN met a larger fraction of the hot water demands, the new heat exchanger enables unused solar energy to feed significant thermal power into the DHN during the day. In Ref. [28], the authors proposed a TRNSYS model evaluating the DHN’s role as solar energy storage. The study found that even distributing solar collectors across buildings maximizes energy production. Additionally, buildings without solar systems can receive a variable share of solar energy (ranging from 34 % to 4 %), depending on their proximity to the nearest solar feed-in point.

The integration of prosumers into low and ultra-low-temperature DHNs was investigated in Ref. [29], showing significant improvements in energy efficiency and heat loss reduction. Utilizing a user-friendly modeling framework, the study revealed that prosumers can decrease overall heat demand to centralized plants by up to 25 %. However, several challenges persist, including the integration of seasonal thermal storage, and the optimal placement of prosumers within the network. In Ref. [30] the authors showed the benefits arising from lowering the operating temperature and introducing bidirectional heat exchange with the DHN: the presence of prosumers and the solar field could lead to a 31.3 % reduction in the energy produced by the centralized plant and a 17.6 % reduction in energy consumed for pumping. A case study regarding a local DHN in Trondheim was replicated in a virtual model [31]. It demonstrated that prosumers, such as data centers and retail stores, significantly reduce heat demand and carbon dioxide emissions. An optimization model was built in Modelica software to analyze distribution temperature in heat-prosumer-based district heating systems, emphasizing the integration of renewable energy sources and thermal energy storage [32]. While the adoption of lower temperatures enhances energy efficiency, it also has an impact on peak load costs. Another optimization analysis of prosumer equipped with storage technology in DHN is presented in Ref. [33]. The results demonstrated that incorporating the water tank thermal energy storage in the prosumer substation reduced the peak load by as much as 39 % while increasing the waste heat self-utilization rate from 79 % to 96 %.

The importance of introducing the prosumer within the district heating markets was discussed in Ref. [34]; the main barriers are referred to as social acceptance and economic regulatory framework. The heat pricing and third-party access should be accurately considered to build a new market structure that fosters prosumer operation. The authors proposed the implementation of a coordination methodology based on a peer-to-peer market without a supervising entity. This showed reliable network solutions, fixing 99.88 % of network burdens and promoting prosumers’ integration. Most heat pricing analysis studies are mainly focused on DHN dealers and investigate the formulation of price from the point of view of a centralized producer [35]. In Ref. [36], the effects of the bidirectional trade of surplus heat between thermal grids on overall operational efficiency were examined. The methodology employed an event-based empirical correlation formulation, which allows for the assessment of new operating conditions without the need for extensive simulations. The results indicated that profits are more sensitive to electricity sales prices than to the heat ones. In Ref. [37], the authors reviewed business models for integration prosumers in DHNs, focusing on flexibility and heat pricing. They identified a diversity of approaches to computing benefits, with marginal cost pricing being the most prevalent. However, the study highlights that marginal cost pricing often neglects investment costs, potentially disincentivizing prosumer participation. A novel community-based transactive market for a 5GDHN with thermal prosumers was proposed in Ref. [38]. The optimization algorithm minimized costs, achieving up to 40 % electricity savings.

1.1. Research gaps and scopes of the work

To fully integrate RES into DHCNs, a deeper understanding of the potential benefits and challenges for both the networks and prosumers is

essential. Based on the literature review, the following gaps have been identified:

- Many studies have explored novel DHNs fueled by large centralized RES plants with a focus on the reduction of fossil fuel consumption and carbon dioxide emissions [39–41]. However, there is a need for a more comprehensive theoretical and modeling framework that includes small-to medium-scale RES producers distributed along a DHN. Indeed, a clear understanding of the technical factors influencing the integration of these heat producers (e.g., pressure distribution along the network) is necessary.
- Although the concept of thermal prosumers is becoming common in research, there is a shortage of studies that characterize the best RES technologies to be used, along with criteria for the design of substations that enable bidirectional heat exchange with DHN. In addition, a detailed analysis of the impact of economic and boundary conditions on the prosumer (e.g., preferring self-consumption or heat sales) is still lacking. In this respect, heat-pricing mechanisms for DHNs with prosumers are absent.
- Few studies analyzed the time profile of heat production from RES prosumers. There is a need to address technical challenges (e.g., ensuring adequate heat temperature for DHN synchronizing heat production with network demand, the necessity of thermal energy curtailment) and economic constraints (e.g., unit heat production cost exceeding the purchase price from the grid). Defining effective strategies to enhance prosumer integration is crucial for advancing RES adoption in DHNs [30,42,43].
- Although several studies present optimistic results in terms of thermal-prosumer integration, there is a knowledge gap regarding the operative modes and criticalities. One of the techno-economic barriers that can hinder effective thermal prosumer development is the availability of the DHN to accept thermal energy by third parties (specifically, the prosumers). Previous studies supposed that the entire amount produced and not used by the prosumers could be delivered to the DHN, but this cannot be true due to several conditions.

On this basis, the present study examines the potential energy and economic benefits for a thermal prosumer equipped with high-vacuum solar collectors in the Mediterranean region. For an office building, the possibility of meeting not only the heating demand but also the cooling one through absorption chillers fueled by the solar plant is investigated. Two different climatic locations in the Mediterranean area were assumed: one with predominant heating demand but lower solar radiation and vice versa. Dynamic simulations are performed by a validated model of a bidirectional substation, with a focus on the heat exchanged by the solar plant, the user, and the DHN. An economic analysis provides insights into the factors that could limit the profitability of the investments. The analysis is replicated for different sizes of the solar plant to investigate the reduction of heat requested by the user to the DHN, the amount of heat that can be transferred to the DHN, and the effects on the unit cost of the heat produced. The following contributions could be identified:

- Insights into the potential use of solar thermal systems as reference technology for prosumers in DHNs are provided. High-vacuum technology is the reference one due to its ability to achieve higher operating temperatures, making it suitable for space heating demands and integration with absorption chillers [44–46]. The effects of the size of the solar plant on the amount of heat available for DHN are quantified, together with the capability of the plant to meet the heating and cooling demand of the prosumer. Through detailed economic analysis, the main factors affecting the profitability of the investment are evidenced.
- A comparative analysis of energy savings and surplus heat available for sale to the DHN is conducted for two different locations in the Mediterranean region. In this context, the study explores the potential for buildings in this area to become thermal prosumers by leveraging solar radiation. It quantifies the amount of heat that could be shared and examines the feasibility of simultaneously meeting cooling demands. In this respect, the impact of incorporating thermally driven cooling systems on energy savings and economic revenues will be analyzed.
- The study will clarify the need to rely on detailed modeling of the thermal prosumer's substation to account for technical constraints that could limit the achievable benefits, e.g., temperature setpoint for the water to be transferred to the supply of the DHN, minimum temperature of the heat from the solar plant for driving absorption chiller.
- Finally, the impact of DHN's ability to absorb surplus thermal energy on investment profitability is analyzed. In this respect, thermal curtailments in thermal energy production are virtually simulated, and the effects on the profitability of the investment and the minimum price of the produced heat are investigated.

The work is organized as follows: Section 2 is dedicated to the description of the reference bidirectional substation and its modeling. In Section 3, the case study is presented together with details on the modeling of reference energy systems (solar plants, electric chiller, and absorption chiller). Furthermore, the energy key performance indicators (KPI), and input data for the economic analysis are detailed. In Section 4, results for typical days in the heating and cooling seasons are first presented, followed by a focus on yearly energy results and limitations of this study. Finally, in Section 5, conclusions are drawn with an analysis of the future perspectives for the research on this topic.

2. Materials and method

Fig. 1 presents a schematic of the bidirectional substation used as the reference system in this study. Originally proposed by Pipiciello et al. [20], this system was later modeled and validated by some of the present paper's authors [25]. As shown in Fig. 1, it is composed of four main subsystems that connect the prosumer substation to the DHN, the heating and cooling generation systems, and the user load. Specifically:

1. The primary circuit that connects the substation to DHN through HE1.
2. The secondary circuit that connects the substation to the user through HE1 and HE2.
3. The tertiary circuit connects the substation to the local heating and cooling generation system through HE2 and HE3.
4. The auxiliary circuits connect the solar collector system, absorption chiller, and storage tanks to the main heat exchangers.

The substation is configured by following the "return-to-supply" model since it ensures more reliability to the thermal system management if compared to the configuration of other thermal prosumer substations [47].

The following systems were included for the generation of thermal and cooling energy:

- High vacuum solar thermal collectors that provide heat to the user during winter and to the absorption chiller generator during summer;
- absorption chiller that supplies cooling during summer and is supplied by solar collectors;
- vapor compression chiller that supplies cooling during summer and operates as a backup of absorption chiller.

Three different operation modes have been set according to seasonal requirements.

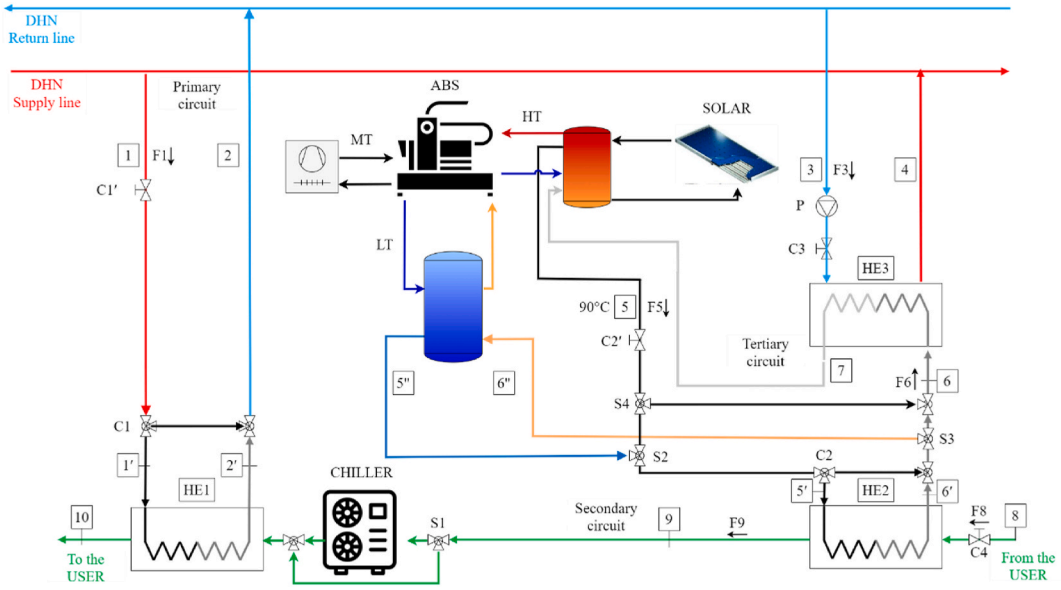

Fig. 1. Layout of the thermo-hydraulic simulated model.

- *Heating mode*: the return user flow is delivered to HE2, where it is heated up by the hot flow coming from the solar system composed of solar collectors and the storage tank. The C2 valve, through a controller, attempts to maintain the temperature outlet on the user line at the required set-point by varying the flow rate on the primary side of HE2. If the available solar energy is not enough to reach the desired temperature set-point, the HE1 is activated. Within this heat exchanger, the user flow exchanges heat with the hot flow coming from the DHN. The flow rate at node 1 is controlled to maintain the T10 temperature at the user set-point by variating the primary flow rate at diverter valve C1. The seasonal S1 valve is opened on the bypass line to skip the vapor compression chiller that is deactivated during winter. If the solar energy available is higher than the user demand, the excess heat is sold to the DHN through the HE3: the feed-in flow is extracted from the return line of the DHN and heated up to the temperature of the supply line by the solar plant. A controller checks the pump speed and modulates the flow rate on node 3 to maintain the desired outlet temperature at node 4, at the interface with DHN. When the user does not request heat, the solar energy is entirely delivered to the HE3 and sold to the DHN.
- *Cooling mode*: through the HE2 the user flow is cooled down by the cold flow coming from the cold tank that is maintained at the desired set point by the absorption chiller. This is activated when the operating conditions occur: heat available for the absorption generator, cooling request on the cold tank, and external temperature within the operating limits admitted. If the summer set-point is not reached, the vapor-compression heat pump is operated to maintain the user cooling request. The C1′ check valve is closed and the HE1 is deactivated. The seasonal valves S2 and S3 let to bypass the HE3 during the cooling operation mode. The solar energy supplies the absorption generator and the HE3 through the seasonal S4 valve that bypasses the HE2, thus avoiding heat-up of the user flow during cooling mode.
- *Intermediate periods*: during the intermediate seasons there is no energy requested by the user, so the entire amount of energy produced by the solar collectors is delivered to the DHN through the HE3. HE1 and HE2 are deactivated, and both chillers are turned off.

2.1. Modelling of the reference bidirectional substation

The system described was reproduced in TRNSYS 17 [48] by replicating the validated model introduced in Ref. [25]. The flexibility of this software enables the modification, addition, and integration of multiple components. Specifically, TRNSYS facilitates the simulation of a substation's transient behavior within a thermal grid, accounting for fluctuations in user demand or variations in distributed heating generation, such as solar thermal production influenced by changing weather conditions. Table 1 reports the list of the TRNSYS types implemented in the model, simulating the main components of the physical setup.

The heat exchangers were modeled by type 5b (counter-flow heat exchangers). Once the specific heat of fluids flowing in the heat exchanger is set, type 5b requires as input the temperature and flow rate of both fluids and the overall heat transfer coefficient (UA). Since the last one is strictly dependent on the flow rate, a constant value was not suitable for this application. As implemented in Ref. [25]. A tailored mathematical model was developed to simulate the dynamic variation of the UA coefficient for each heat exchanger. In particular, knowing the heat transfer coefficient under nominal flow rate conditions UA_n, the aim is to achieve the same coefficient under varied flow rate UA*. The ratio between the heat transfer coefficients is proportional to the Nusselt number ratio that, in this case, can be simply expressed by the Dittus-Boelter expression [49] through Reynolds number (Re) and Prandtl number (Pr):

Table 1
Main TRNSYS type implemented in the model.

Component	TRNSYS Type
Heat Exchanger	Type 5: Counter Flow Heat Exchanger. The overall heat transfer coefficient was calculated externally, following the Logarithmic Mean Temperature Difference method, as presented in [25]
Solar Collector	Type 539: Flat Plate Solar Collector with Capacitance and Flow Modulation
Storage tank	Type 534: Cylindrical Storage Tank with Immersed Heat Exchangers
Absorption chiller and vapor compression chiller	Calculator implementing equations (1)–(6) for absorption, 7–10 for vapor compression. The component's modeling is implemented through a list of equations embedded in the calculator TNRSYS type, thus constituting a generic model.
Controllers	Type 22: Iterative Feedback Controller
Pumps	Type 110: Variable speed pump
Heating and Cooling season scheduler	Type 515 reporting the seasonal schedules according to the Italian law, as shown in Table 3
Multiple Day Scheduler	Type 516
Holiday Scheduler	Type 519

$$Nu = 0.023 Re^{4/5} Pr^{n} \quad (1)$$

Considering that the temperature variation from the nominal conditions is not large (a $|\Delta T| < 30$ °C is typically observed for both hot and cold fluids), it was assumed that $Pr_n = Pr^*$, and the ratio between the UA coefficient is proportional to the Reynolds number ratio.

$$Nu = 0.023 Re^{4/5} Pr^{n} \quad (2)$$

$$\frac{UA_n}{UA^*} = \frac{U_n}{U^*} \cong \frac{Nu_n}{Nu^*} \cong \left(\frac{Re_n}{Re^*}\right)^{4/5} \quad (3)$$

In which the subscript "n" indicates the nominal conditions, and the superscript "*" indicates the conditions under varied flow rates. Finally, a correlation between flow rate and UA was found as follows:

$$\frac{UA^*}{UA_n} = \frac{\left(\frac{m_h^*}{m_{h,n}}\right)^{4/5} \cdot \left(\frac{m_c^*}{m_{c,n}}\right)^{4/5} \cdot \left[1 + \left(\frac{m_{c,n}}{m_{h,n}}\right)^{4/5}\right]}{\left(\frac{m_c^*}{m_{h,n}}\right)^{4/5} + \left(\frac{m_h^*}{m_{h,n}}\right)^{4/5}} \quad (4)$$

where m_h refers to the flow rate on the hot side of the heat exchanger and m_c the cold one. Equation (4) was implemented in a calculator type that, for given nominal and operation flow rates on the hot and cold sides, calculates the overall heat transfer coefficient for each heat exchanger and each simulation time step. This approach gives high flexibility to the model that can be scalable for several applications.

The diverter and mixing valves were modeled by type 11f and type 11h, and the flow rate splitting on the diverter is controlled by an iterative feedback controller (type 22). This controller was implemented to model a real feedback controller (e.g. PID) that would adapt its control signal continuously or use a discrete timestep much shorter than the TRNSYS simulation timestep.

The absorption chiller and the vapor-compression one were modeled by introducing a black box model, described in the following section, implemented in the calculator TRNSYS type.

The solar collector was modeled by adopting the type 539, previously validated in Ref. [50]. This type tries to keep the collector outlet to the outlet set-point temperature by varying the water flow rate. In addition, it shuts off the collector (achieved by setting the water flow rate to zero) if the collector is losing energy. A seasonal control manages the flow delivered to the HE3 to avoid an excessive discharge of the hot storage tank: during the winter period, heat selling to the DHN is permitted when the temperature of the storage tank at the outlet node of the pipeline is higher than 65 °C; during summer this reference temperature is elevated at 80 °C to maintain a thermal level adequate to the absorber generator. The simulation time step was set at 1 h. The sketch of the TRNSYS model is available in the supplementary materials.

3. Case study

In this section, the reference building and its modeling are first described. A detailed description of the main energy plants is given, together with technical details and modeling. Finally, the main input and constraints of this analysis are presented.

3.1. Description of the reference building

A standardized office building from ASHRAE 90.1–2016 [51,52] was adopted for the present analysis. The adopted building is a "medium office", composed of 3 floors, an aspect ratio equal to 1.5, and a window fraction of 33 %. The total conditioned surface and volume are, respectively, 4980 m^2 and 19744 m^3. The thermal properties of the envelope were adapted to the Italian building stock by UNI/TR 11552:2014 [53] and here detailed in Table 2. The building model was developed by combining GOOGLE SKETCHUP (for 3D modeling) with TRNSYS [41].

The analysis was performed by considering two different Italian locations, representative of two different climate zones in the Mediterranean area: Palermo (Csa Köppen-Geiger classification [54]) and Verona (Cfa Köppen-Geiger classification). Specifically, Palermo (Csa) has a hot-summer Mediterranean climate with hot, dry summers (28–34 °C) and mild, wet winters (10–16 °C). Typically, cooling demand is higher than the heating one. Conversely, Verona (Cfa) has a humid subtropical climate with hot, humid summers (18–32 °C) and cool, damp winters (0–8 °C). Consequently, the heating demand is more prevalent than the cooling one.

The climatic data (e.g., outdoor air temperature, solar irradiation, and so on) were retrieved by using the Meteonorm v. 8 database [55], a large database containing historical data retrieved from 8350 weather stations located in all countries. In Fig. 2, the monthly solar radiation and monthly average temperature for both locations are reported. In terms of solar radiation, Palermo shows higher values, with peaks ranging above 225 kWh/m^2 in June and July, whereas Verona reaches a maximum of around 190 kWh/m^2 in the same months. The lowest solar radiation is found in December, with Palermo around 60 kWh/m^2 and Verona below 40 kWh/m^2. As regards air temperature, Palermo maintains a milder climate throughout the year, with winter average

Table 2
Properties of the chosen building according to ASHRAE 90.1 and UNI/TR 11552:2014.

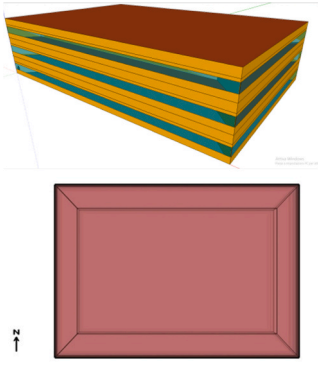

Geometrical properties and internal gains of the building according to ASHRAE 90.1	
Net floor area [m^2]	4982.2
Number of floors	3
Window-Wall-Ratio (WWR) [%]	33
Number of thermal zones	18
Lighting [W/m^2]	11
Electric equipment [W/m^2]	8
Occupants [m^2/person]	19
Thermal properties *worst case* according to UNI/TR 1552: 2014	
Ground [W/m^2K] – Code	1.32 – SOL08
External wall [W/m^2K] – Code	1.42 – MPF01
External roof [W/m^2K] – Code	1.47 – COP04
Adjacent wall [W/m^2K] – Code	2.12 – MLP03
Adjacent ceiling [W/m^2K] – Code	1.68 – SOL02
Windows [W/m^2K] – Code	2.83 –WinID 1002 TRNSYS library

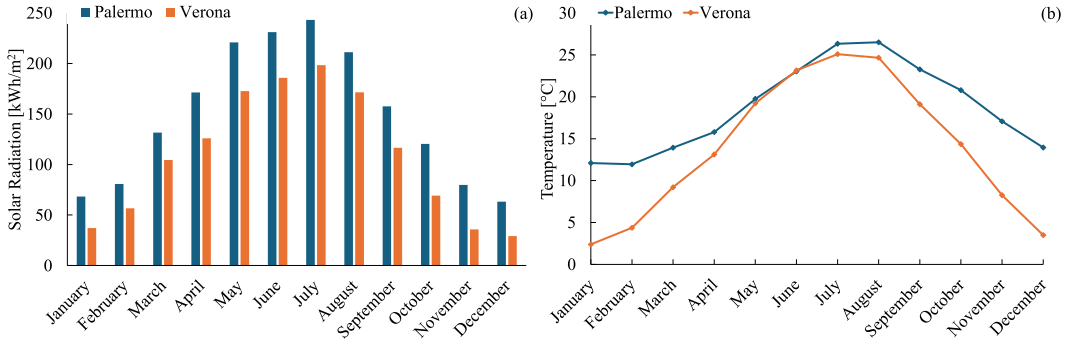

Fig. 2. Monthly solar radiation (a) and monthly average temperature (b) for the selected locations.

temperatures around 12 °C in January and February, gradually increasing to a peak of approximately 27 °C in July. In contrast, Verona exhibits more extreme seasonal variations, with winter temperatures dropping close to 2 °C in January and rising to about 25 °C in July. After summer, both cities experience a gradual decrease in temperature, but Verona cools down more sharply, reaching close to 5 °C by December, while Palermo remains above 12 °C.

These data suggest that due to the different climatic conditions, different results could be found in terms of the amount of heat from solar energy that could be sold to DHN during the heating season and also the fraction of the cooling demand that could be covered by the thermally driven chiller.

The heating and cooling periods were set according to Italian regulation [56], which also identifies 6 different climatic zones according to the standard degree days. The climatic zones are classified from zone A (hottest) to F (coldest); the selected locations belong to zones B (Palermo) and E (Verona) [57]. In Table 3, the heating and cooling periods adopted for the simulation are reported.

Worth mentioning that the Russian-Ukrainian war and the uncontrolled increase in energy prices led the Italian government to reduce the heating period. The periods not included in the heating or cooling ones are here indicated as “intermediate seasons”.

Infiltration (air infiltration allowance air changes/h), lighting, electrical equipment, and internal gains from people were defined based on separate time schedules by month and day of the week, as specified by ASHRAE 90.1–2016 and here reported in the Supplementary File.

To calculate the hourly heating and cooling demands of the building (which are then used to size the heating and cooling plants), the “ideal plant” option in TRNSYS was used. This routine assumes the existence of an air-conditioning plant that is capable of always maintaining the required indoor temperature setpoint (i.e., 20 °C in winter and 26 °C in summer) [48]. The selected time step for calculating the building demand was 1 h.

Fig. 3a-b show the hourly profile of the space heating and cooling for Palermo and Verona, respectively. Looking at Fig. 3a, the heating demand for Palermo shows a 131.8 kW peak, reached in the coldest period of the winter season. In Verona (Fig. 3b), the winter hourly profile shows higher values, due to the different climates, and ranging up to 316 kW. The space cooling demand profile shows an opposite behavior with demand peaks reaching 236.1 kW for Palermo (Fig. 3a), and 186.7 kW for Verona (Fig. 3b).

Table 3
Definition of the heating and cooling periods adopted for the simulation [56].

	Palermo	Verona
Heating period	From 08th December to 23rd March for a maximum of 7 h per day	From 22nd October to 7th April for a maximum of 13 h per day
Cooling period	No restrictions – from 01st June to 30th September	No restrictions – from 01st June to 30th September

Fig. 3c shows the monthly heating and cooling energy for both locations. The resulting values are 27.7 MWh and 73.3 MWh, respectively for the yearly heating and cooling energy in Palermo, and 168.8 MWh and 71.9 MWh, respectively for the yearly heating and cooling energy in Verona.

Note that domestic hot water was not included in this analysis due to the predominance of the energy demand due to air conditioning typically observed in office buildings [58].

3.2. Data on the solar plant and the bidirectional substation

The solar thermal system is composed of high vacuum solar collectors TVP Solar MT whose data, retrieved from the European Certification “Solar Keymark” [59], are reported in Table 4.

The heat exchangers’ nominal size (i.e. UA) was selected according to the operating temperatures of both the DHN and the hydronic loop within the building. The nominal values used to size the heat exchangers are reported in Table 5 (the readers are invited to refer to Fig. 1 to properly locate the flows and temperatures collected in this table). The nominal duty of each heat exchanger (Q) was calculated through the energy balance, using the nominal water flow rate (F) and temperature in Table 5. The UA values were then determined by using the logarithmic mean temperature difference according to Nusselt’s method. Specifically, for the DHN, return and supply temperatures of 40 °C and 60 °C were taken into consideration, respectively. These temperature values comply with the definition of 3rd DHN generation, close to the 4th, as suggested in Ref. [60]. The user load return temperature (T8) ranges between 40 °C (maximum demand) and 50 °C (no demand) for winter and 12 °C (maximum demand) and 7 °C (no demand) for summer. The solar collector nominal set point was fixed at 95 °C, but for the heat exchanger sizing, the temperature inlet was set respectively at 80 °C for HE2 (T5′) and 95 °C for HE3 (T6). The difference between T5′ and T6 relies on the conservative approach implemented to ensure the correct size of HE2 even in case of lower temperatures than the nominal expected, as occurs during winter.

3.3. Description of the reference absorption chiller

The reference absorption chiller is a single-effect LiBr-H_20 manufactured by “Baelz” [61], a German company with expertise in energy-saving solutions for industry and buildings. More specifically, the “Bumblebee model” characterized by a nominal cooling capacity of 160 kW was selected, with some data collected in Table 6. Note that the column “Hot Circuit, HT” indicates the temperature of the hot water provided to the generator of the absorption chiller together with the water flowrate), which is supplied by the solar plant. The column “Cooling Circuit, MT” indicates the temperatures and flow rate of water used to cool down the condenser and the absorber. Finally, the “Cold circuit, LT” indicates the temperature and flow rate of water returning (and supplied) from (to) the hydronic loop of the buildings.

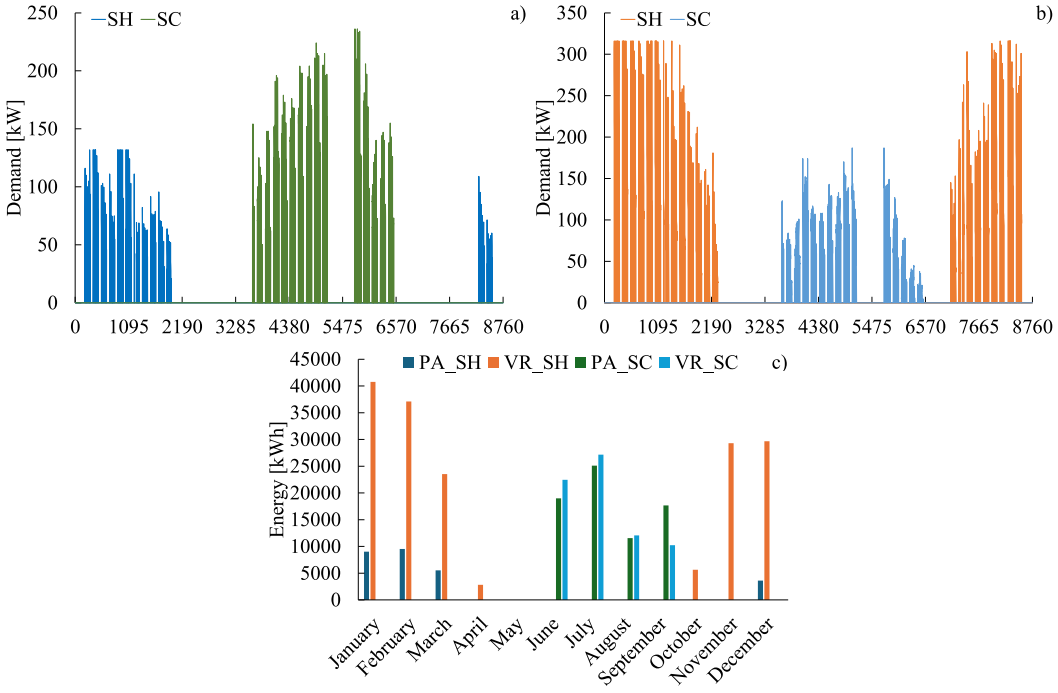

Fig. 3. Heating (SH) and Cooling (SC) demands for (a) Palermo, (b) Verona. (c) Monthly values of the heating and cooling energy for both selected locations.

Table 4
Solar Keymark Parameter of the chosen high vacuum solar thermal panel.

Parameter	Value	Unit
Gross Area A_G	1.96	m^2
Zero loss efficiency (η_0)	0.732	
First-order coefficient (a_1)	0.5	W/m^2K
Second-order coefficient (a_2)	0.006	W/m^2K^2
Incidence angle modifier IAM (50°)	0.95	
Heat transfer medium for testing	Water	
Maximum temperature difference for thermal performance calculation $(\theta_m\text{-}\theta_a)_{max}$	185	K
Standard stagnation temperature (G = 1000 W/m^2, θ_a = 30 °C)	302	°C
Effective thermal capacity, including fluid (per gross area A_G)	15.32	$kJ/K\ m^2$
Maximum operating temperature	200	°C
Maximum operating pressure	160	kPa

The same chiller was selected for both locations since it could meet the cooling demand of reference buildings for 75.3 % of cooling hours in Palermo and 98.5 % in Verona. As previously shown (see Fig. 1), the absorption chiller is connected to a storage tank whose volume was calculated as suggested by Ref. [62]. A 3,000-L storage tank was estimated.

A "black box approach" was adopted to model the operation of the absorption chiller [63]. More specifically, Eqs (5) and (6) were used to quantify the COP, the delivered cooling capacity ($\dot{Q}_{ev,abs}$), and the mass flow rate of the hot water supplied to the generator ($\dot{m}_{HT}$) by knowing (i) the temperature of the water returning the hydronic loop of the building and entering the evaporator of the absorption chiller (i.e., LT_{in}), (ii) the temperature of the water used to cool down the condenser (MT_{in}), and (iii) the temperature of the water supplied to the generator of the absorption chiller, coming from the solar plant (H_{tin}). The $f_{\dot{Q}_{ev,abs}}$ in Eq. (7) is the part load ratio of the chiller (i.e., the ratio with the actual cooling capacity delivered and the nominal value $\dot{Q}_{ev,abs,nom}$). To evaluate the fitting coefficients "a_i", "b_i", and "c_i", experimental data from the datasheet of the chiller were used. Then, by using the "Curve Fitter" tool available in MATLAB software, a non-linear regression was performed to calculate the fitting coefficient "a_i" and "c_i" in Eqs (5) and (7), and a linear regression for "b_i" in Eq. (7). Once the COP and cooling capacity are known, the energy balance equations of the absorption chiller are used to calculate the thermal power requested by the generator ($\dot{Q}_{g,abs}$, Eq. (9)) and the energy delivered to cooling water flowing in the condenser ($\dot{Q}_{c,abs}$, Eq. (10)).

$$COP = \frac{a_1 \cdot HT_{in}^2 + a_2 \cdot HT_{in} + a_3}{HT_{in} + a_4} \tag{5}$$

$$\dot{Q}_{ev,abs} = b_1 + b_2 \cdot HT_{in} + b_3 \cdot MT_{in} + b_4 \cdot LT_{in} \tag{6}$$

$$\dot{m}_{HT} = \frac{c_1 \cdot f_{\dot{Q}_{ev,abs}} + c_2}{f^2_{\dot{Q}_{ev,abs}} + c_3 \cdot f_{\dot{Q}_{ev,abs}} + c_4} \tag{7}$$

$$f_{\dot{Q}_{ev,abs}} = \frac{\dot{Q}_{ev,abs}}{\dot{Q}_{ev,abs,nom}} \tag{8}$$

$$\dot{Q}_{g,abs} = \frac{\dot{Q}_{ev,abs}}{COP} \tag{9}$$

$$\dot{Q}_{c,abs} = \dot{Q}_{ev,abs} + \dot{Q}_{g,abs} \tag{10}$$

The full list of fitting coefficients is available in the Supplementary Materials. The accuracy of the regression was evaluated by using the R-squared (R^2), the root mean square error (RMSE), and the sum of squares error (SSE). As shown in Table 7, high values of R^2 (close to 1) and low values for SSE and RMSE were found, suggesting the capability of the model to approximate data from the datasheet. Fig. 4 shows the matching between the experimental data retrieved by the datasheet and the numerical data obtained by the model.

3.4. Description and modeling of the reference vapor-compression chiller

The nominal capacity of the air-cooled chiller was selected to cover the peak in the cooling demand for each location. In this respect, chillers from the Italian company "Aermec" company [64] were used. As shown in Table 8, 237.3-kW chiller was selected for Palermo and a 187.7-kW

Table 5
Design of the heat exchangers in the substation. HE1: Heat Exchanger 1 (Fig. 1) – HE2: Heat Exchanger 2 (Fig. 1) – HE3: Heat Exchanger 3 (Fig. 1) – F1: Flow rate drawn from district heating network - T1': Temperature of flow drawn from district heating network (inlet temperature of Heat Exchanger 1 primary side) - T2': Outlet Temperature from Heat Exchanger 2 primary side – T9: Outlet Temperature of the secondary side of Heat Exchanger 2 (user side) - F9: Flow Rate of user side – T10: Outlet Temperature from Heat Exchanger1 secondary side (user side) – F5: Flow Rate outlet from heating generation plant (solar collector field) - T5: Inlet Temperature of the Heat Exchanger 2 (supply side) – T6': Outlet Temperature of the primary side of Heat Exchanger 2 (supply side) – T8: Inlet temperature of the secondary side of Heat Exchanger 1 (demand side) – F3: Flow rate drawn from district heating network in the producer mode – T3: Inlet temperature of the secondary side of Heat Exchanger 3 (demand side) – T4: Outlet Temperature of the secondary side of Heat Exchanger 3 (demand side) – F6 Inlet Flow Rate on the primary side of Heat Exchanger 3 (supply side) - T6: Inlet temperature of the primary side of Heat Exchanger 3 (supply side) – T7: Outlet Temperature of the primary side of Heat Exchanger 3 (supply side).

Heat exchanger	Palermo case				Verona case			
	Primary side		Secondary side		Primary side		Secondary side	
HE1	F_1 7558	l/h	F_9 11336	l/h	F_1 18122	l/h	F_9 27182	l/h
	$T_{1'}$ 60	°C	T_9 40	°C	$T_{1'}$ 60	°C	T_9 40	°C
	$T_{2'}$ 45	°C	T_{10} 50	°C	$T_{2'}$ 45	°C	T_{10} 50	°C
	Q 132	kW			Q 316	kW		
	UA 11.33	kW/°C			UA 43.82	kW/°C		
HE2	F_5 5668	l/h	F_8 11336	l/h	F_5 13591	l/h	F_8 27182	l/h
	T_5 80	°C	T_8 40	°C	T_5 80 °C	°C	T_8 40	°C
	$T_{6'}$ 60	°C	T_9 50	°C	$T_{6'}$ 60 °C	°C	T_9 50	°C
	Q 132	kW			Q 316	kW		
	UA 5.34	kW/°C			UA 12.82	kW/°C		
HE3	F_3 7085	l/h	F_6 5668	l/h	F_3 16988	l/h	F_6 13591	l/h
	T_3 40	°C	T_6 95	°C	T_3 40	°C	T_6 95	°C
	T_4 60	°C	T_7 70	°C	T_4 60	°C	T_7 70	°C
	Q 165	kW			Q 395	kW		
	UA 5.08	kW/°C			UA 12.18	kW/°C		

Table 6
Nominal data for the "Bumblebee" absorption chiller.

Hot circuit (HT)	Cooling circuit (MT)	Cold circuit (LT)
Nominal Inlet temperature 90 °C	Nominal Inlet temperature 30 °C	Nominal Inlet temperature 21 °C
Outlet temperature 72 °C	Outlet temperature 37 °C	Outlet temperature 16 °C
Volume flow rate 9.6 m^3/h	Volume flow rate 44.2 m^3/h	Volume flow rate 27.5 m^3/h
Heating capacity 200 kW	Heat consumption 360 kW	Cooling capacity 160 kW
Type	Single effect LiBr-H_2O	
Cooling Capacity	160 kW	
Coefficient of performance (referring to the reported nominal temperature conditions)	0.80	
T_{min} (hot water/cold water)	60 °C/5 °C	
T_{max} (cooling water)	40 °C	
Power consumption	Max 700W	

one for Verona. The design data retrieved from the manufacturer are shown in Table 8. The models NRG0802X°TU°J°00 for Palermo and NRB0702°TU°M°00 for Verona were retrieved from the selection tool provided by the company.

A black box approach was again adopted for modeling these chillers.

Table 7
Evaluation of the accuracy of the model of the absorption chiller. SSE: Sum of Squared Errors – R^2: Coefficient of determination – RMSE: Root Mean Square Error – COP: Coefficient Of Performance, $Q_{ev,abs}$: Cooling capacity at the evaporator of absorption chiller - $\dot{m}_{HT}$: Flow rate on absorption chiller's generator loop (High Temperature).

	COP	$Q_{ev,abs}$	$\dot{m}_{HT}$
SSE	0.0001	8169	2.48
R^2	0.974	0.993	0.998
RMSE	0.009	3.33	0.170

Specifically, as shown in Eqs. (11) and (12), the EER and cooling capacity ($\dot{Q}_{ev,comp}$) are dependent on the temperature of the outdoor air entering the condenser (T_{air}) and the temperature of the water returning from the hydronic loop and entering the evaporator of the chiller ($T_{w,in}$). The energy balance of the chiller lets to calculate the power requested by the unit (P_{el}, Eq. (13)), including the compressor and condenser fan, and the energy delivered to the condenser ($\dot{Q}_{c,comp}$, Eq. (14)). To evaluate the fitting coefficients "a_i" and "b_i", experimental data from the datasheet of the chiller were used. Then, by using the "Curve Fitter" tool available in MATLAB software, the fitting coefficients were quantified.

$$EER = a_1 + a_2 \cdot T_{air} + a_3 \cdot T_{w,in} \tag{11}$$

$$\dot{Q}_{ev,comp} = b_1 + b_2 \cdot T_{air} + b_3 \cdot T_{w,in} \tag{12}$$

$$P_{el} = \frac{\dot{Q}_{ev,comp}}{EER} \tag{13}$$

$$\dot{Q}_{c,comp} = \dot{Q}_{ev,comp} + P_{el} \tag{14}$$

The full list of fitting coefficient values "a_i" and "b_i" is again provided in the Supplementary Materials. In Table 9, the High values of R^2 and low values of RMSE suggest the capability of the model to approximate data from the datasheet. Figs. 5 and 6 provide details on the matching between the experimental data retrieved from the datasheet and the numerical data obtained from the regression model.

3.5. On the need to perform a sensitivity analysis

With reference to the nominal operating conditions indicated in the datasheet and Solar Keymark certificate, the nominal size of the solar collectors was selected to cover the peak heating demand. However, to explore the effects of solar energy exploitation on energy savings and profitability, four different scenarios were simulated, each characterized by a different size of the solar plants: 100 % (nominal size), 75 %, 50 %, and 25 % of nominal size. Each string is composed of 14 collectors, and for this reason, the partial design collector surface was set to the closest theoretical value. The solar collector system is connected to a storage tank that was sized according to the recommendation reported in Ref. [65], by considering the minimum ratio between storage volume and solar surface fixed to 0.05 m^3/m^2. Table 10 shows the simulation input for each scenario. For each solar system size, a simulation scenario was run to assess the influence of solar energy availability.

The control logic attempts to reach the cooling water temperature outlet at 7 °C, which was the fixed supply user set-point.

A quadratic correlation between the flow rate ratio and the electrical power of the solar circulating pump is found for each scenario (Table 11).

3.6. Energy key performance indicators

A set of Key Performance Indicators (KPIs) is introduced to compare the different scenarios and the effect of the different locations. Specifically, $f_{sol,w}$ (Eq. (15)) represents the fraction of the heating demand

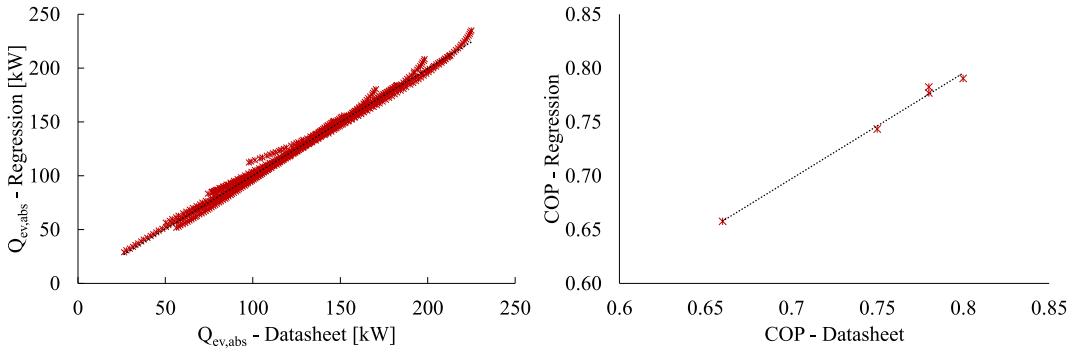

Fig. 4. Comparison between performance data obtained by data sheet and regression numerical model for the absorption chiller.

Table 8
Air-to-water chiller design operating data.

		Palermo	Verona
Cooling Capacity	kW	237.3	187.7
Power absorbed (included condenser fan)	kW	74.1	57.9
EER	[−]	3.20	3.24
Dry bulb ambient air temperature	°C	35	35
Water inlet temperature	°C	12	12
Water outlet temperature	°C	7	7
Water flow rate	l/s	11.32	8.94
Water Pressure Drop	kPa	80	54
Current absorbed	A	119.8	100.5
Refrigerant	[−]	R23	R410A
Compressor Type	[−]	Scroll	Scroll
Number of compressors	[−]	2	2

Table 9
Evaluation of the accuracy of the black box model of the vapor compression chiller. SSE: Sum of Squared Errors – R^2: Coefficient of determination – RMSE: Root Mean Square Error – EER: Energy Efficiency Ratio - $Q_{ev,comp}$: Cooling capacity at the evaporator of compression chiller – PA: Palermo – VR: Verona.

	EER_PA	EER_VR	$Q_{ev,comp}$_PA	$Q_{ev,comp}$_VR
SSE	1.227	0.668	21.59	50.14
R^2	0.924	0.943	0.999	0.999
RMSE	0.269	0.198	1.127	1.717

($\dot{Q}_{load,w}$) covered by heat from the solar system ($\dot{Q}_{HE2,w}$). $f_{DHN,w}$ (Eq. (16)) represents the complement to $f_{sol,w}$ and it is the fraction of heating demand covered by the DHN ($\dot{Q}_{HE1}$). $f_{abs,s}$ (Eq. (17)) represents the fraction of cooling demand ($\dot{Q}_{load,s}$) covered by the absorption chiller ($\dot{Q}_{ev,abs}$). ε_{solar} (Eq. (18)) represents the efficiency of solar collectors expressed as the ratio between the thermal energy produced by the collectors ($\dot{Q}_{solar}$) and the solar radiation incident (I_{tilt}) on the tilted surface ($A_{sol,tilt}$) of the collectors. COP_{abs} (Eq. (19)) represents the "average" performance of the absorption chiller, calculated as the ratio between the cooling energy produced at the evaporator ($\dot{Q}_{LT}$) and the heating energy demand of the generator during the entire cooling season ($\dot{Q}_{HT}$). Finally, the EER (Eq. (20)) is the "average" energy efficiency ratio of the vapor compression chiller expressed as a ratio between the cooling energy produced at the evaporator ($\dot{Q}_c$) and the electrical energy absorbed by the compressor and the condenser fan during the entire cooling season (P_{el}).

$$f_{sol,w} = \frac{\int_{ti}^{tf} \dot{Q}_{load,w}\, dt}{\int_{ti}^{tf} \dot{Q}_{HE2,w}\, dt} \tag{15}$$

$$f_{DHN,w} = \frac{\int_{ti}^{tf} \dot{Q}_{load,w}\, dt}{\int_{ti}^{tf} \dot{Q}_{HE1}\, dt} \tag{16}$$

$$f_{abs,s} = \frac{\int_{ti}^{tf} \dot{Q}_{ev,abs}\, dt}{\int_{ti}^{tf} \dot{Q}_{load,s}\, dt} \tag{17}$$

$$\varepsilon_{solar} = \frac{\int_{0}^{8760} \dot{Q}_{solar}\, dt}{A_{sol,tilt} \cdot \int_{0}^{8760} I_{tilt}\, dt} \tag{18}$$

$$COP_{abs} = \frac{\int_{ti}^{tf} \dot{Q}_{LT}\, dta}{\int_{ti}^{tf} \dot{Q}_{HT}\, dt} \tag{19}$$

$$EER = \frac{\int_{ti}^{tf} \dot{Q}_c\, dta}{\int_{ti}^{tf} P_{el}\, dt} \tag{20}$$

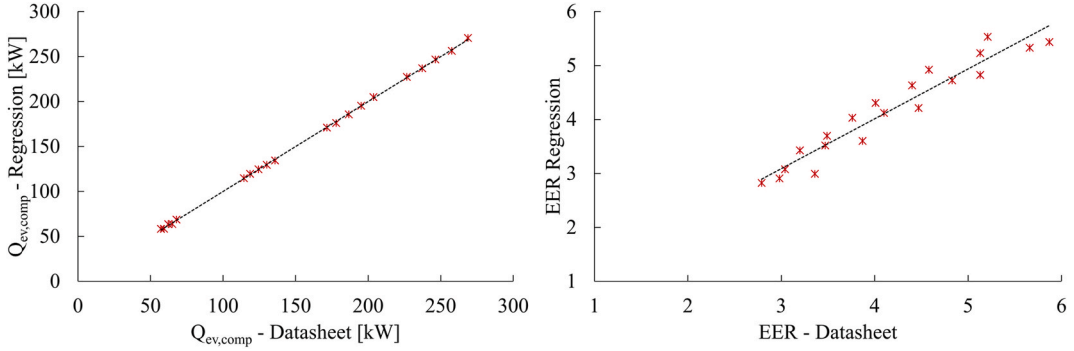

Fig. 5. Comparison between performance data obtained by data sheet and regression numerical model for Palermo vapor compression chiller. *$Q_{ev,comp}$: Cooling capacity at the evaporator of compression chiller.*

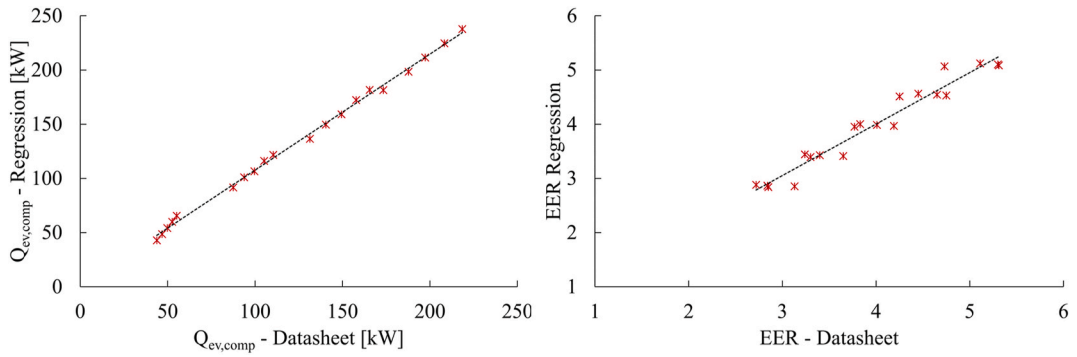

Fig. 6. Comparison between performance data obtained by data sheet and regression numerical model for Verona vapor compression chiller. $Q_{ev,comp}$: Cooling capacity at the evaporator of compression chiller.

Table 10
Solar collector and storage tank design scenarios.

Ratio of nominal size	Palermo				Verona			
	Solar collectors' surface		Storage tank volume		Solar collectors' surface		Storage tank volume	
Nominal size (100 %)	231	m^2	11.5	m^3	514	m^2	25.7	m^3
75 %	180	m^2	9	m^3	385	m^2	19.3	m^3
50 %	128	m^2	6.4	m^3	257	m^2	12.9	m^3
25 %	51	m^2	2.6	m^3	128	m^2	6.4	m^3

3.7. Economic analysis

To evaluate the feasibility of investments, the Net Present Value (NPV) was assumed and calculated according to Eq. (21),

$$NPV = \sum_{i=0}^{N} \frac{CF_i}{(1 + WACC)^i} \tag{21}$$

where CF is the cash flow in the "i-th year", WACC is the Weighted Average Cost of Capital, and "N" is the expected lifetime of the system. The WACC estimation is mainly related to the technology proposed.

The economic analysis was carried out considering that the described system was introduced as a retrofit within an existing baseline system. The baseline system comprises the same user that DHN entirely supplies for the heating demand and the vapor compression chiller for the cooling one.

The cash flow (CF) was calculated as indicated in Eq. (22), by the difference between the yearly Operation Expenditure costs (OPEX) of the baseline system compared to one of the simulated scenarios, plus the income obtained by selling heat to the network (I_{th}). In this respect, OPEX considers both the purchase of electricity and heat and the maintenance costs.

In Eq. (23), Q_{HE3} is the total amount of heat exchanged by the HE3, and p_{sell_DHN} is the selling price of heat to the DHN.

$$CF_i = I_{th} + \left(OPEX_{baseline} - OPEX_{scen.i}\right) \tag{22}$$

$$I_{th} = Q_{HE3} \cdot p_{sell\_DHN} \tag{23}$$

3.7.1. Details on capital and operating expenditure costs

The estimation of CAPEX of the solar collector system (including pipelines and auxiliaries), absorption chiller, thermal storage, and the costs that should be sustained to change the substation layout from heat consumer to prosumer. As previously mentioned, OPEX is composed of two components: maintenance costs and operating costs. The reference year for all monetary values indicated in this study is 2022. Specifically:

- The CAPEX of the solar collector is affected by the size of the proposed system, which is considerably higher than the small system for single house application for DHW (<10 m^2) and, conversely, lower than the solar district heating application (>1000 m^2). The market references are given for the two aforementioned applications, and an average estimation was performed due to the size range of the current analysis. The Danish Energy Agency releases yearly the market trend for a wide set of technologies; for the solar collector technology, the costs range between 320 €/m^2 and 470 €/m^2 [66]. The International Renewable Energy Agency (IRENA) reports a range variable from 409 USD/kW to 1000 USD/kW for some European Countries [67]. Considering the nominal efficiency of the selected solar collector technology (η = 0.68), the technology of the collector (high vacuum), and the high performance declared by manufacturers, the estimated CAPEX for the present analysis was 500 €/m^2. For the solar system, the yearly maintenance costs are estimated at a fixed tariff of 250€ plus a cost proportional to the collector's surface: 1 €/m^2 [66]. The operating costs of the solar system are related to the electricity consumption to supply the circulating pump and the dry cooler operated to dissipate the excess heat during the eventual moments of thermal grid curtailment, i.e., situations during which the grid dealer cannot receive the excess heat from the prosumer. In these cases, to avoid the overheating of the collectors, a safety dry cooler is operated.
- The absorption chiller CAPEX was estimated by considering several sources. In Ref. [68] a solar-coupled absorption system was presented; the CAPEX of the absorption chiller was 472 €/kW (referred to as the cooling nominal capacity). In Ref. [69] an absorption chiller was coupled with a Fresnel solar plant with a specific cost of 288 €/kW, in Ref. [70] a CAPEX ranging between 314 and 571 €/kW is reported with an Operation and Maintenance cost of 0.17 €/kWh

Table 11
Correlation between the flow rate ratio of the solar system and electrical power [kW] of the circulating pump.

Flow rate ratio	Palermo				Verona			
	231 m^2	180 m^2	128 m^2	51 m^2	514 m^2	385 m^2	257 m^2	128 m^2
25 %	0.163	0.135	0.135	0.026	0.105	0.093	0.17	0.135
50 %	0.301	0.188	0.188	0.099	0.599	0.505	0.324	0.188
75 %	0.910	0.567	0.567	0.282	1.876	1.560	0.986	0.567
100 %	2.095	1.317	1.317	0.631	4.381	3.623	2.276	1.317

(cooling), comprehensive of electricity needed to activate the circulating pumps. Considering the range explored and the maturity of the technology, the CAPEX selected for the present study is 411.6 €/kW, with a maintenance cost of 0.05 €/kWh, the first referring to the nominal cooling capacity and the second to the cooling energy produced for one year.

- For the assessment of the thermal storage CAPEX, the large volume should be considered. Analogous to the solar system, the selected sizes are among the most usual sizes recognized by the market: the domestic tanks with a volume that usually does not exceed 0.5 m^3 and large storage tanks used for district heating systems, whose volume typically is higher than 1000 m^3. The European Association for Storage of Energy, for the selected size range, suggests 1200 €/m^3 [71]. An installation of a high-stratification storage tank performed within the SunHorizon project [72] showed a CAPEX of approximately 1500 €/m^3. Also in this case, an average value of 1350 €/m^3 was estimated.
- Finally, the installation cost for expanding the substation should be considered. A substation equipped with a single heat exchanger (simple consumer) is installed in the reference case. The simulation takes into account a substation equipped for the prosumer operation with three heat exchangers and the relative auxiliaries (piping, valves, circulator, sensors, etc.). The Danish Energy Agency [73] presents a range varying between 30 and 70 €/kW. The first value refers to the substation whose nominal capacity is analog to those implemented in the present study, so that value was adopted as reference CAPEX.

Table 12 reports the summary of the specific costs assumed for CAPEX calculation.

A summary of Investment Costs is indicated in Table 13. The impact of the solar system on the overall CAPEX is the most relevant in almost all cases. When the solar collector surface is lower, the relevance decreases, and the absorption chiller has a higher weight (45 % and 63 % for Palermo – 128 m^2 and 51 m^2 for the absorption chiller versus 43 %, 25 % for solar system). The storage and substation have a lower weight on the total investments, equal to 12 % for Palermo and ranging between 15 % and 18 % for Verona.

3.7.2. Further data for the economic analysis

The assumed value for WACC introduced in Eq. (21) was defined by considering the analysis performed in 2022 for Heating Companies and Heat Exchangers in the Netherlands actively operating in the field of District Heating. Based on those market references, WACC is fixed at 4.23 %, and N = 20 years [74].

The purchasing prices of electricity and heat are indicated in Table 14. Specifically, the price of electricity was estimated by considering both Italian electricity prices for 2023 presented by Eurostat (non-domestic users, yearly consumption ranging between 20 and 500 MWh) [75]. These data are also confirmed by the Italian Regulatory Authority for Energy, Networks, and Environment (ARERA) [76].

The price of heat was retrieved from the 2023 price list released by the company that manages the DHNs for the municipality of Verona [77]. A yearly average price was calculated by considering the monthly variation presented by the company for the user that requests less than 29 MWh per month.

Table 12
Specific cost assumed for CAPEX.

Technology	Specific cost assumed for Economic Analysis (CAPEX)		Reference
Solar collectors	500	€/m^2	[66,67]
Absorption chiller	411.6	€/kW	[68–70]
Thermal Storage Tank	1350	€/m^3	[71,72]
DHN prosumer substation	30	€/kW	[73]

Regarding heat selling prices, to maximize income I_{th} (see Eq. (23)), it was first assumed that all excess heat generated by the solar system was sold at the same price as the purchased heat. Then, a sensitivity analysis was carried out by varying Q_{HE3} and p_{sell_DHN} (Eq. (22)). Indeed, in a real system, the DHN manager could not accept the total amount of the heat available from the prosumer (i.e., Q_{HE3}), due to several factors (low demand, unavailability to partialize the centralized heat generators, hydraulic interferences, etc.). Therefore, a thermal curtailment occurs (analogously to the electrical grid with RES), and the prosumer must dissipate the surplus heat produced by the solar collectors when the storage is full. In these cases, the activation of a safety dry-cooler to avoid the superheating and stagnation of collectors is required, with a further cost to be sustained. In the economic analysis, a curtailment ratio (%cur) ranging from 0 to 100 % was considered. This value means that the DHN manager accepts all the heat released by the HE3 for 0 % curtailment and cuts off all the heat available in the case of 100 % curtailment. Meantime, the p_{sell_DHN} (the price of heat sold to the DHN) was varied between 0 % and 100 % p_{DHN} (the price of heat purchased to the DHN), to explore the whole range of p_{sell_DHN} that can be negotiated between the prosumer and the DHN manager and its effects on the economic profitability in a long-term perspective.

4. Results and discussion

To provide insights into system operation, the results are presented at multiple scales, from hourly profiles on two representative days to annual energy balances. Finally, the key findings from the economic analysis are discussed.

4.1. Focus on daily results

Focusing on Palermo, January 30th is selected as the reference day for the heating season, while July 10th for the cooling one. Note that, for the sake of brevity, the discussion is limited only to the results for two solar field sizes: 230 m^2, representing the reference configuration, and 126 m^2, corresponding to 50 % of the nominal area.

Fig. 7 shows the hourly profiles of the thermal power exchanged within each heat exchanger for the reference heating and cooling days. Looking at Fig. 7a and b, it is possible to observe that during the first part of the day (07:00 a.m. - 01:00 p.m.), the thermal power exchanged between the solar system and the user via HE2 is higher in the case of 230 m^2 solar field, as shown by comparing the orange profiles in Fig. 7a and b. Consequently, the thermal power exchanged between the user and the DHN via HE1 is reduced. In the second part of the day, when the energy stored in the solar tank is higher and the user demand is lower, the building acts as a producer, selling surplus heat to the DHN through HE3, as testified by the green profiles in Fig. 7a and b. Notably, higher values are found in the case of a 230 m^2 solar field, as testified by comparing the peak in thermal power sold to the DHN, respectively equal to 97 kW and 53 kW.

In the reference cooling day (Fig. 7c and d), the solar energy delivered to the absorption chiller (red profiles) is maximum in the first half of the morning and afternoon, with some oscillations for the case of 126 m^2 solar field due to the thermostat activation. A 150-kW peak in the heat sold to the DHN is observed in the case of a 230 m^2 solar field at around 1:30 p.m. when there is no cooling demand from the user. Conversely, no peak was observed in the case of a 126 m^2 solar field. In the remaining part of the day, the amount of heat sold to the grid is not continuous, with some oscillation due to thermostat action, which must ensure higher temperatures to comply with the absorption chiller's minimum temperature; for this reason, when the hot tank reaches the lower setpoint, the F7 flow is interrupted.

Focusing on Verona (see Fig. 8), the reference days are March 21st and July 25th. Even in this case, during the heating season (Fig. 8a and b), the HE1 mostly operates in the first part of the day (06:00–12:00 a.m.) when the solar radiation is lower and the user demand is at its

Table 13
Investment costs for the simulated scenarios.

		Palermo				Verona			
		231 m^2	180 m^2	128 m^2	51 m^2	514 m^2	385 m^2	257 m^2	128 m^2
Solar collectors	[k€]	115.5	90	64	25.5	257	192.5	128.5	64
Thermal Storage	[k€]	155.3	12.2	8.6	3.5	34.7	26.1	17.4	8.6
Absorption chiller	[k€]	65.9	65.9	65.9	65.9	65.9	65.9	65.9	65.9
Substation	[k€]	8.9	8.9	8.9	8.9	21.4	21.4	21.4	21.4
TOTAL CAPEX	[k€]	**205.8**	**176.9**	**147.4**	**103.8**	**378.9**	**305.8**	**233.2**	**159.8**

Table 14
Unit Price of energy vectors.

	Price		Reference
Electricity	0.2044	€/kWh	[75,76]
Heat (from DHN)	0.1786	€/kWh	[77]

maximum. Moreover, comparing Fig. 8a with 8.b, the effect of solar collector size is evident between 06:00 a.m. and 12:00 a.m., as suggested by the higher values of the thermal power exchanged within HE2 for the 514 m^2 case. In the second part of the day (01:00 p.m.–06:00 p.m.), similar profiles are found for the selected collector sizes, thus indicating that the solar energy produced and stored in the previous hours is enough to cover the user demand.

As shown in Fig. 8a, a 514 m^2 solar field achieves a peak thermal output of 175 kW through HE3, demonstrating the potential to export surplus heat to the DHN and operate as a thermal prosumer. Conversely, as shown in Fig. 8b, an oscillating profile is also found in this case of lower solar collect size. Finally, within the same sizing case, it is possible to observe that HE1 compensates for the lack of energy available for the user in the last part of the day.

In the typical cooling day (Fig. 8c and d), the absorption chiller operates nearly all day (as shown by the HT profile in Fig. 8c and d), from early morning to late evening, ensuring a continuous supply of cooling energy to the cold storage. This results in noticeable differences between the two selected cases: in the case of a solar field surface of 514 m^2, more heat is available and, consequently, more cooling can be produced by the absorption chiller.

Looking at the thermal power exchanged in HE3, it is evident that the user is a prosumer all day, including at nighttime. In addition, when the solar collector surface is equal to 514 m^2, the amount of heat sold to the grid is higher.

Fig. 9 shows the temperature of the solar collector and HE2 in Palermo and Verona during the reference winter day. To point out the main limitation of the system, results found for the minor solar collector surface are plotted for both cases (i.e., 51 m^2 for Palermo and 128 m^2 for Verona). Focusing on Palermo (Fig. 9a), due to the low temperature in the tank, the user flow outlet (T9) does not achieve the temperature set-point (i.e., 50 °C) during the first part of the day, thus requiring the DHN supply. In the second half of the day, the available temperature of the flow delivered from the tank to the HE2 primary side inlet rises to 70 °C, thus guaranteeing the required energy and meeting the temperature setpoint.

A similar behavior is observed in Verona (Fig. 9b), where the storage tank, having been fully discharged the previous day, must accumulate sufficient energy during the initial hours of the reference day to ensure that the user-side flow temperature reaches the required setpoint. In both cases, although the temperature of the flow coming from the storage tank is not enough to cover the whole demand, it acts as a

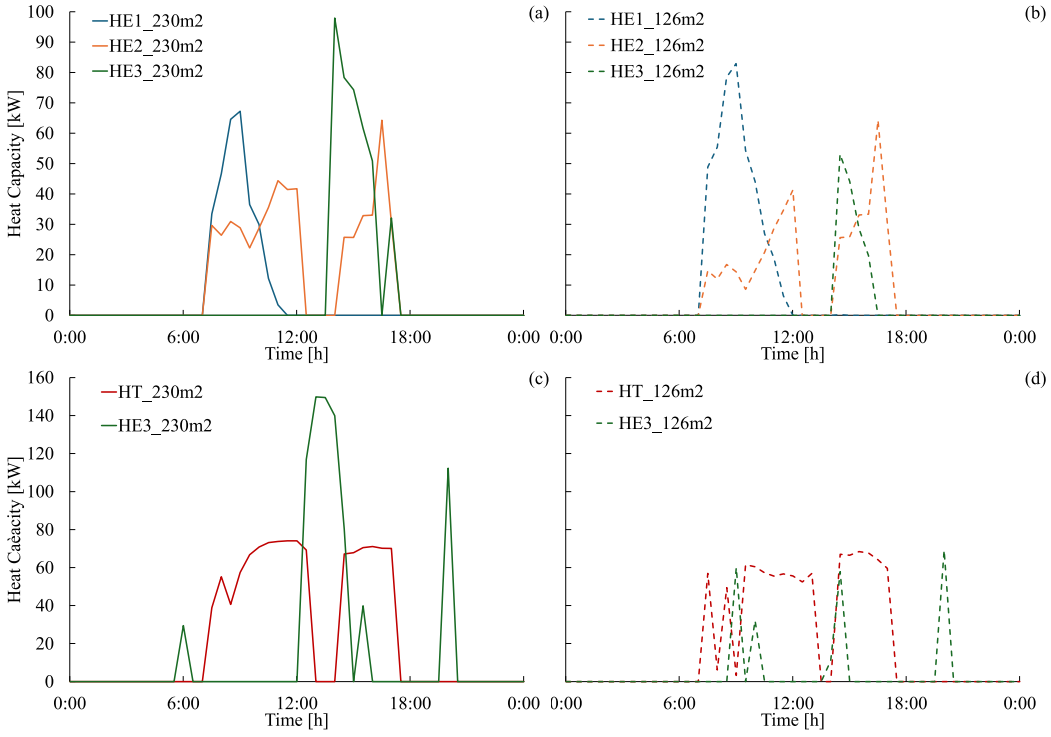

Fig. 7. Profile for a reference day in Palermo. a) Winter day 230 m^2 – b) Winter day 126 m^2 – c) Summer day 230 m^2 – d) Summer day 126 m^2. HE1: Heat Exchanger 1 (Fig. 1); HE2: Heat Exchanger 2 (Fig. 1); HE3: Heat Exchanger 3 (Fig. 1); HT: Temperature inlet on the absorption chiller's generator loop (High Temperature).

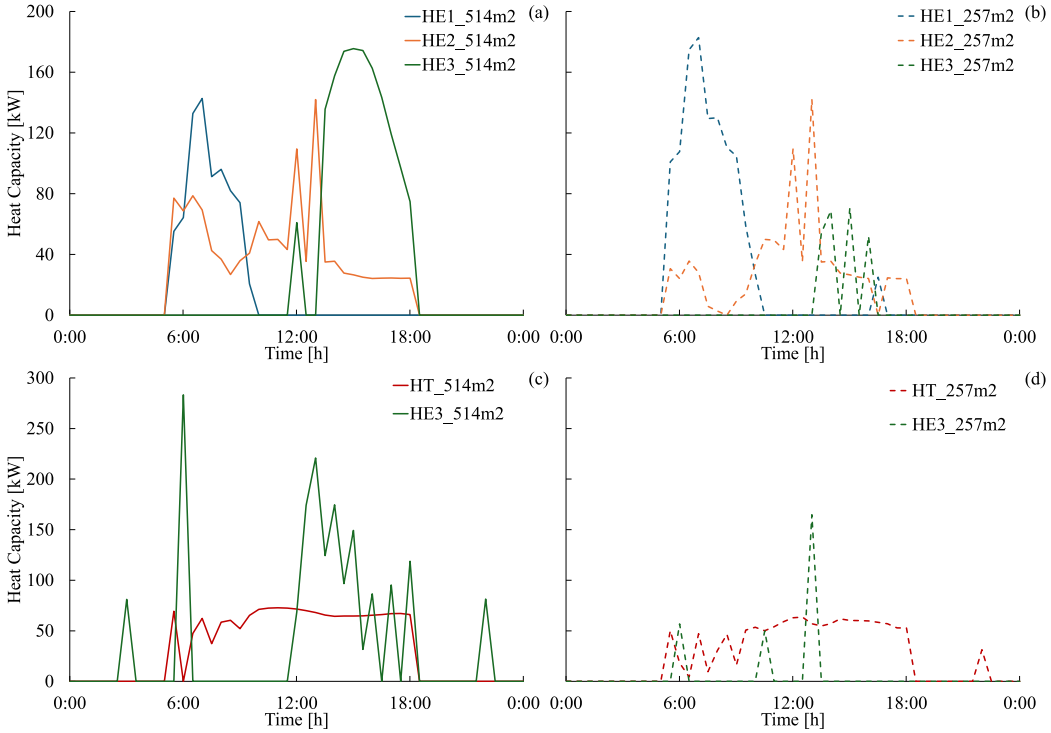

Fig. 8. Profiles for a reference day in Verona. a) Winter day 514 m^2 – b) Winter day 257 m^2 – c) Summer day 514 m^2 – d) Summer day 257 m^2. HE1: Heat Exchanger 1 (Fig. 1); HE2: Heat Exchanger 2 (Fig. 1); HE3: Heat Exchanger 3 (Fig. 1); HT: Temperature inlet on the absorption chiller's generator loop (High Temperature).

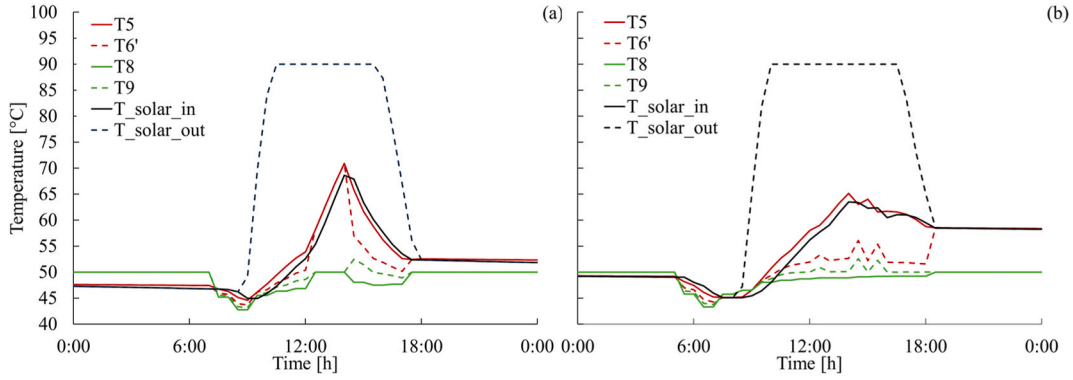

Fig. 9. temperature profile of the solar collector system and HE2 for Palermo (a) and Verona (b) for the reference winter day. For both cases, the minor solar collector surface scenario was chosen. T5 Inlet temperature of the primary side of Heat Exchanger 2 (Supply side, Fig. 1) – T6': Outlet Temperature of the primary side of Heat Exchanger 2 (Supply side, Fig. 1) - T8: Inlet temperature of the secondary side of Heat Exchanger 1 (Demand side, Fig. 1) – T9: Outlet Temperature of the secondary side of Heat Exchanger 1 (Demand side, Fig. 1) – T_solar_in: Inlet Temperature of the solar collectors – T_solar_out: Outlet Temperature of the solar collectors.

preheater, lowering the energy requested from the DHN. Finally, an increase in the surface area of the solar field leads to a higher share of energy demand being met by solar energy.

Fig. 10 shows the daily profile of cooling power from HE2 and vapor compression chiller during the reference cooling day in Palermo (Fig. 10a) and Verona (Fig. 10b). In Fig. 10a, the influence of solar system sizing on the cooling capacity provided via HE2 by the absorption chiller is evident. In the second part of the day, the difference between the two cases becomes less pronounced, as the heat stored in the morning is sufficient to drive the absorption chiller. In both scenarios, the vapor compression chiller provides approximately twice the cooling capacity of the absorption chiller.

Focusing on Verona (Fig. 10b), the differences between the first and second part of the day are less marked. Since a lower amount of heat is available for operating the absorption machine, lower cooling capacity is exchanged via HE2. As can be noted, the differences in cooling capacity between the two sizing scenarios range between 10 kW and 20 kW. Again, the compression chiller supplies most of the cooling load requested by the user.

4.2. Yearly energy results

Starting from the case of Palermo, Fig. 11 shows the energy balance of the substation and the solar plant. More specifically, the ratio between the energy transferred by each HE and the total energy exchanged within the substation is presented. As shown in Fig. 11a, the heat produced by the solar system and supplied to the user via HE2 represents the maximum contribution to the overall energy exchanged for the two intermediate sizes (i.e., 75 % and 50 %), accounting respectively for 41 % (19.1 MWh) and 40 % (15.6 MWh). For the nominal size of the solar field, the predominance of energy produced by the solar system and fed into the DHN via HE3 is evident. In comparison, for the 25 % case, heat

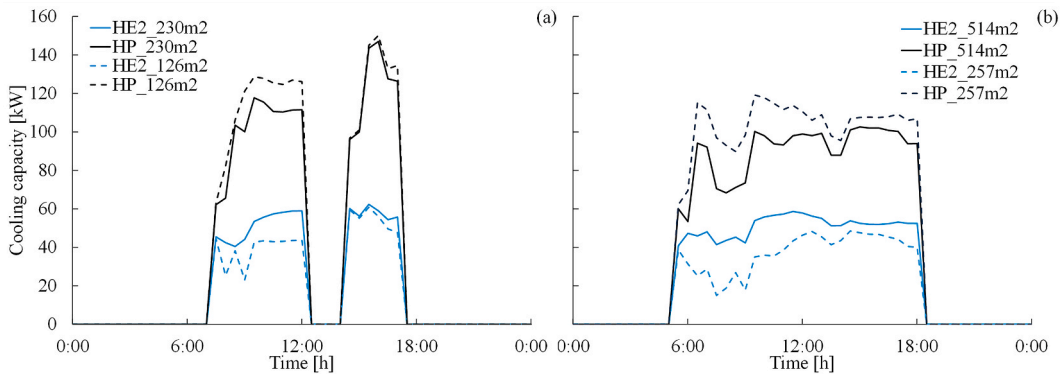

Fig. 10. Profile of cooling capacity exchanged by HE2 and vapor compression HP during summer mode for the selected days: Palermo (a), Verona (b). HE2: Heat Exchanger 2 – HP: Heat Pump.

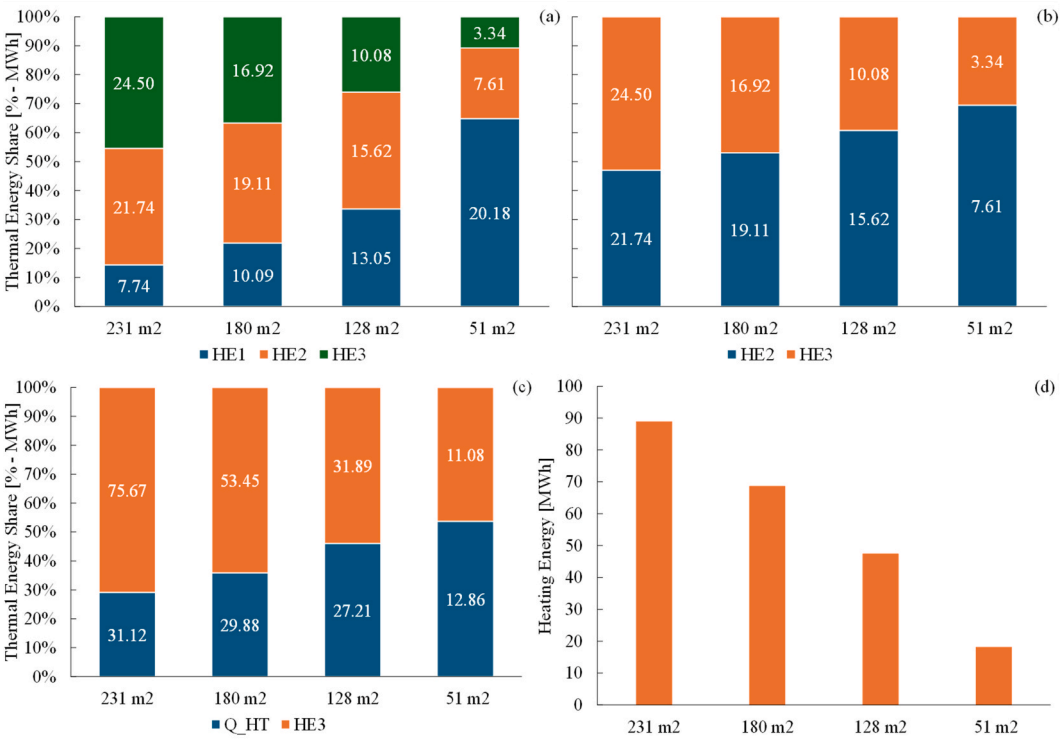

Fig. 11. Energy balance (kWh) of the substation in Palermo. a) Energy distribution among the three heat exchangers in winter, b) energy sharing of the amount of energy produced by the solar system in winter, c) energy balance of the substation and solar system during summer, d) energy balance of the substation and solar system during intermediate seasons. HE1: Heat Exchanger 1 – HE2: Heat Exchanger 2 – HE3 Heat Exchanger 3 – Q_HT: Absorption chiller generator's heat requested.

exchanged through HE1 is predominant, thus representing the need to purchase heat from the DHN, due to the undersized solar system. The energy distribution ratio among the three heat exchangers shows a linear variation for the first three scenarios. Conversely, for the scenario with 25 % size, the HE1 energy share increases steeply, reaching 64.8 % (20.2 MWh). Fig. 11b shows the fraction of the heat produced by the solar system, which is either supplied to the user (HE2) or delivered to the DHN (HE3). It is worth noting that the main contribution belongs to DHN (53 % - 21.7 MWh for HE3) only in the 100 % sizing scenario (230 m^2). In the three scenarios that involve an undersized solar system, most of the heat produced by the solar system is supplied to the user through HE2. This information is useful for optimizing the design of the solar system.

During the summer (Fig. 11c), the heat produced by the solar system is delivered to the absorption chiller (Q_HT) and the DHN. It is worth noting that the fraction of heat from the solar plant supplied to the absorption chiller increases linearly as the solar collector surface decreases, compared to the heat exchanged via HE3. Specifically, the absolute value rises from 12.9 MWh to 31.1 MWh. In addition, for the 100 %, 75 %, and 50 % of nominal size scenarios, most of the energy produced by the solar system is transferred to the DHN. Only in the last scenario, solar energy is equally shared between the absorption chiller and the DHN.

In the intermediate seasons (Fig. 11d), when solar energy is entirely delivered to the DHN, a decreasing trend in exchanged energy is observed — from 88.9 MWh down to 18.1 MWh as the solar field area decreases from 231 m^2 to 51 m^2.

Energy results for the heating season in Verona show significant differences compared to the previous case. As shown in Fig. 12, the contribution of HE1 is predominant over the other heat exchangers (Fig. 12a), thus revealing that DHN is essential for almost all of the winter, regardless of the size of the solar plant. Moreover, as shown in

Fig. 12b, the amount of heat supplied to DHN via HE3 is limited in all cases. Specifically, the share of energy produced by the solar system ranges from 28.6 % (27.4 MWh) for the nominal size to 14.9 % (3.8 MWh) for the minimum size.

The energy results for the cooling season (Fig. 12c) show that the heat transferred to the DHN exceeds the amount supplied to the absorption chiller. This trend is consistent across all scenarios. It is worth noting that the absolute value of Q_HT decreases, highlighting that despite the significant excess energy produced, the solar system is not oversized. For the intermediate season (Fig. 12d), a similar trend to the case of Palermo was observed for the absolute energy supplied to the thermal grid. Although the solar collector surface areas differ substantially between the two cases, this discrepancy is due to variations in solar irradiation and the duration of the operating periods.

In all cases, the bidirectional configuration allows meeting the demand when the solar energy is not enough and avoids dissipating the excess heat produced when there is no request from the loads (user or absorption chiller).

4.3. Key-performance-indicators: results

Table 15 collects the KPIs for the prosumer located in Palermo. The fraction of the heating demand covered by solar energy, $f_{sol,w}$, linearly decreases when the size of the solar plant decreases from 231 m^2 to 128 m^2. A sharp decrease is observed in the last case (i.e., 51 m^2) as the solar system is not able to meet the desired temperature setpoint of the hot water to be supplied to the building. The fraction of heating demand covered by the DHN ($f_{DHN,w}$) complements the previous value, ranging from 26.2 % to 72.6 %. This indicates that even in a location with a mild winter, a significant portion of heating energy is still supplied by the DHN. The fraction of cooling demand covered by the absorption chiller ($f_{abs,s}$) shows a slight decrease in the first three cases (from 231 m^2 to 128 m^2) and a drastic decrease in the last one (i.e., 51 m^2) due to the inability of the solar system to heat water at the temperature required for the correct operation of the absorption machine. The solar efficiency, ε_{solar}, is approximately constant with a slight increase in the case of 51 m^2 due to the higher temperature lift between the inlet and outlet of the collectors. The absorber COP maintains constant values for the first three cases and shows a relevant decrease in the last one due to the lack of thermal energy to supply the absorber. Finally, the EER of the compression chiller maintains a stable level despite the increase in cooling demand when passing from the first to the last case.

Table 15
KPI for the prosumer located in Palermo. **$f_{sol,w}$**: Fraction of the heating demand covered by heat from the solar system - **$f_{DHN,w}$**: fraction of heating demand covered by the DHN (complement to $f_{sol,w}$) - **$f_{abs,s}$**: represents the fraction of cooling demand covered by the absorption chiller - **ε_{solar}**: efficiency of solar collectors expressed as the ratio between the thermal energy produced by the collectors and the solar radiation incident on the tilted surface of the collectors – **COP**: average performance of the absorption chiller, calculated as the ratio between the cooling energy produced at the evaporator and the heating energy demand of the generator during the entire cooling season – **EER**: average energy efficiency ratio of the vapor compression chiller expressed as a ratio between the cooling energy produced at the evaporator (and the electrical energy absorbed by the compressor and the condenser fan during the entire cooling season.

KPI	231 m^2	180 m^2	128 m^2	51 m^2
$f_{sol,w}$	73.8 %	65.5 %	54.5 %	27.4 %
$f_{DHN,w}$	26.2 %	34.5 %	45.5 %	72.6 %
$f_{abs,s}$	33.6 %	32.1 %	28.7 %	12.3 %
ε_{solar}	52.8 %	53.2 %	53.2 %	54.5 %
COP_{abs}	0.79	0.79	0.77	0.70
EER	4.6	4.6	4.6	4.6

The KPIs for Verona (Table 16) reveal that, despite the solar sizing adapted to the peak demand, the fraction of the heating demand covered by solar energy during the heating season (i.e., $f_{sol,w}$) is about 50 % lower in all sizing cases if compared to Palermo. In this context, the presence of DHN is necessary since its load-covering fraction ($f_{sol,w}$) ranges from 61 % to 87.1 % when passing from the maximum to the minimum solar collector size. Conversely, the fraction of the cooling demand covered by the absorption chiller is greater than the one found for Palermo, revealing that such a system can offer valid support even in the cooling period; the $f_{abs,s}$ slightly decrease when passing from 514 m^2

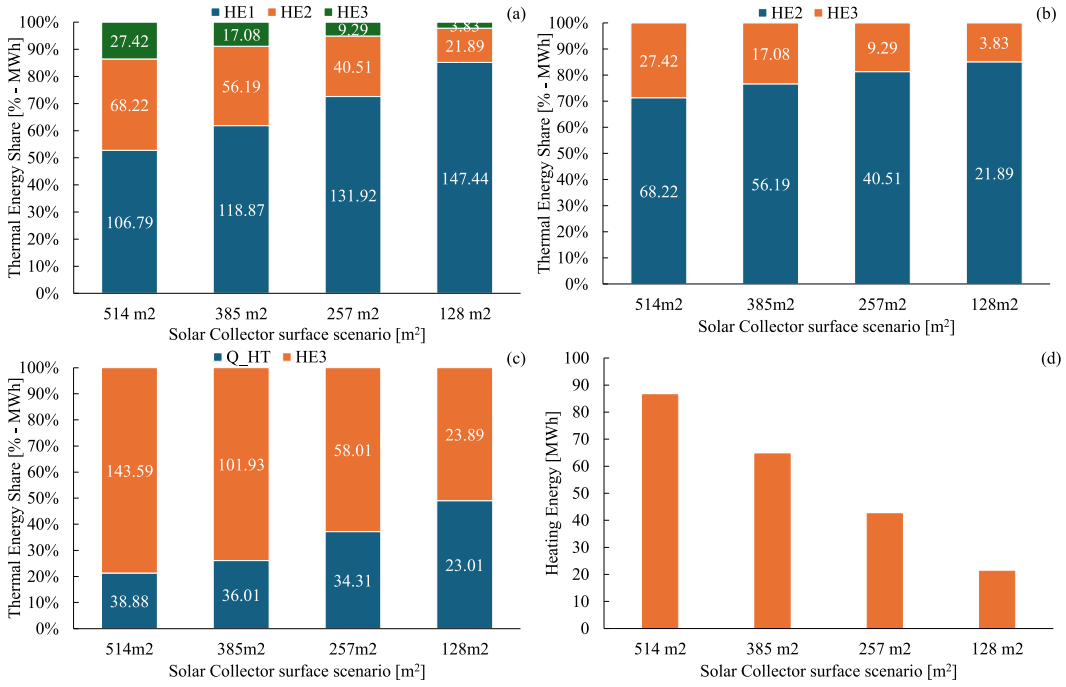

Fig. 12. Energy balance (kWh) of the substation in Verona. a) Energy distribution among the three heat exchangers in winter, b) energy sharing of the amount of energy produced by the solar system in winter, c) energy balance of the substation and solar system during summer, d) energy balance of the substation and solar system during intermediate seasons. HE1: Heat Exchanger 1 – HE2: Heat Exchanger 2 – HE3 Heat Exchanger 3 – Q_HT: Absorption chiller generator's heat requested.

Table 16
KPI for the prosumer located in Verona. **$f_{sol,w}$**: Fraction of the heating demand covered by heat from the solar system - **$f_{DHN,w}$**: fraction of heating demand covered by the DHN (complement to $f_{sol,w}$) - **$f_{abs,s}$**: represents the fraction of cooling demand covered by the absorption chiller - **ε_{solar}**: efficiency of solar collectors expressed as the ratio between the thermal energy produced by the collectors and the solar radiation incident on the tilted surface of the collectors – **COP**: average performance of the absorption chiller, calculated as the ratio between the cooling energy produced at the evaporator and the heating energy demand of the generator during the entire cooling season – **EER**: average energy efficiency ratio of the vapor compression chiller expressed as a ratio between the cooling energy produced at the evaporator (and the electrical energy absorbed by the compressor and the condenser fan during the entire cooling season.

KPI	514 m^2	385 m^2	257 m^2	128 m^2
$f_{sol,w}$	39.0 %	32.1 %	23.5 %	12.9 %
$f_{DHN,w}$	61.0 %	67.9 %	76.5 %	87.1 %
$f_{abs,s}$	43.0 %	39.3 %	37.1 %	23.6 %
ε_{solar}	49.3 %	49.7 %	49.9 %	50.7 %
COP_{abs}	0.80	0.78	0.78	0.74
EER	4.3	4.3	4.3	4.3

to 257 m^2 case, then it undergoes a drastic reduction.

The solar efficiency is nearly constant for all size scenarios. Conversely, the COP of the absorption chiller decreases noticeably only for the minimum solar plant size. Finally, the EER is constant for all the considered solar sizing, although the amount of cooling load covered by the absorption chiller increases complementary to $f_{abs,s}$.

4.4. Economic analysis results

The OPEXs of the baseline scenario were calculated by considering that the heating demand is entirely supplied by the DHN, while the cooling demand is covered by the existing vapor compression chiller (Table 17). The climatic differences are evident when looking at energy expenditure costs. Indeed, in Palermo, the cost sustained for electricity to activate the chiller has a share of 39.4 % on OPEX. Conversely, for Verona, the impact of electricity cost on OPEX is limited (10.1 %), due to the predominant heating demand. In both cases, the expenditure costs for purchasing heat are the most relevant: 63.6 % for Palermo and 89.9 % for Verona.

The yearly OPEX costs for the different sizing scenarios are reported in Table 18. Electricity purchase is the most relevant in the case of Palermo, ranging between 53.8 % and 43.8 %. In addition, the cost sustained for purchasing heat from the DHN increases when the solar collector surface is reduced, passing from 20.4 % to 46.3 %. Finally, for a 51 m^2 solar field, electricity and heat contribute almost equally to the overall OPEX.

For the prosumer located in Verona, the heat purchase mostly contributes, from 76.1 % to 84.3 %. In addition, it is worth noting that the OPEX for Verona is almost three times higher than the ones found for Palermo, due to the higher demand for heating.

Table 19 shows the variation in OPEX and the maximum yearly income achievable for each simulated scenario. Note that I_{th} contribution is predominant on the yearly balance. Although the cost to purchase electricity is higher in the simulated scenarios compared to the baseline (see Table 17), the CF is higher than zero thanks to the heat savings achieved by the solar collectors.

Table 17
Operation expenditure costs of the baseline scenario.

		Palermo	Verona
Electricity	[k€]	3.23	3.41
Heat (from DHN)	[k€]	4.94	30.2
Total OPEX	[k€]	8.17	33.6

4.4.1. Effects of thermal energy curtailment on profitability

An NPV matrix was developed for each scenario by using Matlab R2023b. This matrix shows the variation of NPV achieved by varying the curtailment ratio (%cur) and the price of heat sold to the DHN (p_{sell_DHN}). A map of the NPV for the thermal prosumer in Palermo with 231 m^2 solar collectors is shown in Fig. 13. The results for the remaining scenarios are collected within the Supplementary Materials file.

Looking at the Figure, on the x-axes, the price of the heat sold to the DHN is expressed as a percentage of the purchase price of the heat. On the y-axes, the "$\%_{cur}$" represents the curtailment ratio. In addition, the line with an NPV = 0 marks the boundary between profitable and unprofitable investments. Then, the intersection between the zero-NPV line and x-axes (red line in the figure) represents the minimum selling price of heat, which makes the investment profitable (in this case, equal to 0.435, i.e. 43.5 %). Conversely, the intersection of y-axes zero-NPV line (0.584 in the figure) represents the maximum allowable curtailment ratio, which makes the investment profitable (in this case, equal to 58.4 %).

Table 20 collects intercepts of the zero-NPV curve for all the simulated scenarios. Note that the profitability of the investment decreases when the collector's surface is reduced, as testified by the increase in the p_{sell_DHN} ($\%p_{DHN}$). This is a consequence of the lower incomes arising from selling heat to the grid. In addition, even in the best case (i.e., Palermo – 231 m^2 and Verona 514 m^2) the minimum allowable selling price ratio is high (respectively 43.5 % and 45.4 % of the purchasing price) since it is referred to a limit condition that marks the passage between profitability and no (i.e. NPV = 0). To better explain this, looking at Fig. 13, to obtain an NPV equal to 100 k€ after 20 years, the heat must be sold at a price higher than 66 % of the purchasing price. Consequently, the DHN manager should buy from the prosumer at that price and sell at p_{DHN} with a very low profit margin. A similar consideration can be made for the maximum curtailment limit required for profitability. Since curtailment can occur due to both technical and economic factors, an increase in the heat selling price may lead to a higher curtailment ratio.

Finally, in the scenario with the smallest solar collector surface (i.e., 51 m^2 for Palermo and 128 m^2 for Verona), NPV values remain negative across all conditions.

4.4.2. Effects of the absorption chiller on system profitability

Comparing the electricity cost between the baseline (Table 17) and simulated scenarios (Table 19) reveals that the proposed technologies do lead to great benefits in terms of electricity expenditure costs. As shown in Tables 15 and 16, the KPIs for the absorption chiller indicate a low coverage of cooling demand in the simulated case, suggesting that the investment in this technology does not provide significant economic benefits. However, the cost of heat supply from the grid is reduced across all scenarios. On this basis, a further analysis with no absorption chiller included was conducted for each location. This evaluation was performed only for the maximum solar collector's surface.

Results in Table 21show that the investment costs are reduced, and the expenditures for electricity supply are slightly higher than the baseline (due to the auxiliaries of the substation and solar system), The overall OPEX is lower since the maintenance cost of the absorption chiller is avoided, along with the cost to purchase heat from the DHN, analogously to the aforementioned scenarios. Finally, a higher amount of heat is potentially available to be sold to the grid, since the thermal energy produced during the summer is no longer supplied to the absorption chiller. Higher CF is found than the previous cases, but the income I_{th} is lower. A percentage comparison with the corresponding scenarios that include the absorption chiller is given.

The NPV indicator (Fig. 14) shows relevant improvements if compared to the previous scenarios because of lower investment costs and higher cash flows. Then, avoiding the absorption chiller ensures better economic performance, and as shown in Table 22, the zero–NPV front moves to lower values of $p_{sell,DHN,}$ and higher values of $\%_{cur}$. It

Table 18
OPEX values results (maintenance and operating costs).

		Palermo				Verona			
		231 m^2	180 m^2	128 m^2	51 m^2	514 m^2	385 m^2	257 m^2	128 m^2
Maintenance	[k€]	1.74	1.64	1.46	0.76	2.35	2.08	1.87	1.25
Electricity Purchase	[k€]	3.63	3.33	3.40	3.40	3.68	3.51	3.49	3.62
Heat Purchase	[k€]	1.38	1.80	2.33	3.60	19.1	21.2	23.6	26.3
TOTAL OPEX	[k€]	**6.76**	**6.77**	**7.19**	**7.77**	**25.1**	**26.8**	**28.9**	**31.2**

Table 19
OPEX variation, Maximum yearly incomes, and Cash Flows (CF) achievable for each scenario.

		Palermo				Verona			
		231 m^2	180 m^2	128 m^2	51 m^2	514 m^2	385 m^2	257 m^2	128 m^2
(CF) $OPEX_{baseline}$-$OPEXs_{cenario}$	[k€]	1.41	1.40	0.98	0.40	8.46	6.75	4.65	2.36
I_{th}	[k€]	33.8	24.8	16.0	5.81	46.0	32.8	19.6	8.73
CF	[k€]	**35.2**	**26.2**	**17.0**	**6.21**	**54.4**	**39.5**	**24.2**	11.1

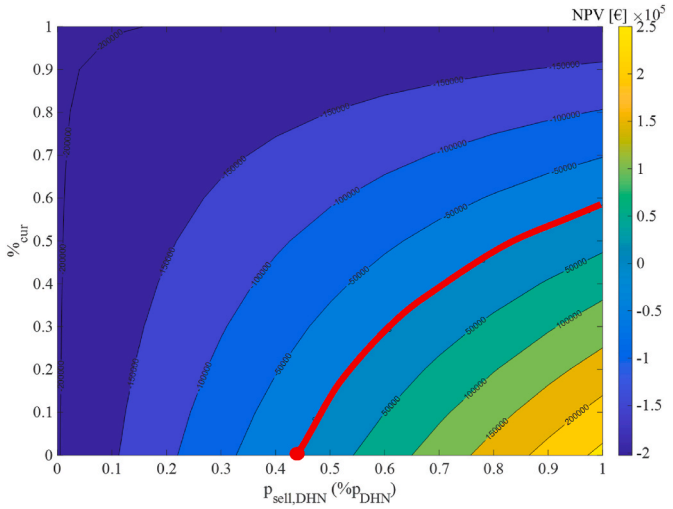

Fig. 13. NPV behavior map for Palermo - 231 m^2 scenario. NPV: Net Present Value - %cur: Curtailment Ratio – $p_{sell,DHN}$: price of heat sold to the grid expressed as a ratio of price purchased by the grid.

follows that profitability is ensured even when the market conditions are critical, i.e. in the case of lower selling price and a high curtailment ratio.

4.5. Limitations of the study

Before ending, it is worth pointing out the main limitations of the present research, which could open a window for future studies on this topic. Specifically:

- Although the study relied on validated models for the bidirectional substation and high-vacuum solar collectors, the overall integrated modeling could not be validated against experimental data due to the absence of existing bidirectional substations coupled with this technology. Future research will need to focus on validation, which will become feasible once experimental setups are available.
- Another limitation is related to the approach used for simulating thermal curtailment. As proven by the results, curtailment highly influences profitability and the set of technologies that could be included within the substation (e.g., the absorption chiller). Then, a co-simulation approach that includes information on DHN status, such as the actual demand for heat from other users, is needed.
- An optimization study will be necessary for the cost-effective sizing of the solar plant and chiller absorption. The sensitivity analysis performed here was not intended to provide information on the optimal size but to provide a preliminary assessment of the effects of this variable on energy savings and economic profitability. Moreover, further analyses should also account for (i) future variability in key parameters such as energy prices, maintenance costs, or government subsidies, (ii) uncertainties in users' heating and cooling demands, and (iii) efficiency degradation over time due to fouling of heat exchangers.
- Another limitation of the study is the lack of consideration for a financing framework that supports both the initial investment and the realization of potential economies of scale. Future analyses should therefore explore the impact of incentivization mechanisms on the system's profitability, as well as assess how economies of scale might influence performance. Additionally, caution must be

Table 21
Main economic indicators for the scenarios without absorption chiller. In brackets, the percentage ratio between the new result and the analog one belonging to the previous scenarios including the absorption chiller.

		No-Absorption Chiller			
		Palermo-231 m^2		Verona 514 m^2	
CAPEX	[k€]	140	(68.0 %)	313.0	(82.6 %)
OPEX	[k€]	5.91	(87.4 %)	24.1	(96 %)
$OPEX_{baseline}$-$OPEX_{scenario}$	[k€]	2.26	(159 %)	9.47	(112 %)
I_{th}	[k€]	39.4	(116 %)	53.2	(115 %)
CF	[k€]	41.7	(118 %)	62.7	(115 %)

Table 20
Values of intercept between the zero - NPV front and axes. %cur: Curtailment Ratio – $p_{sell,DHN}$: price of heat sold to the grid expressed as ratio of price purchased by the grid.

	Palermo				Verona			
	231 m^2	180 m^2	128 m^2	51 m^2	514 m^2	385 m^2	257 m^2	128 m^2
p_{sell_DHN} (%p_{DHN}) -(NPV=0)	0.435	0.496	0.644	/	0.454	0.511	0.668	/
$\%_{cur}$ - (NPV=0)	0.584	0.521	0.368	/	0.565	0.506	0.344	/

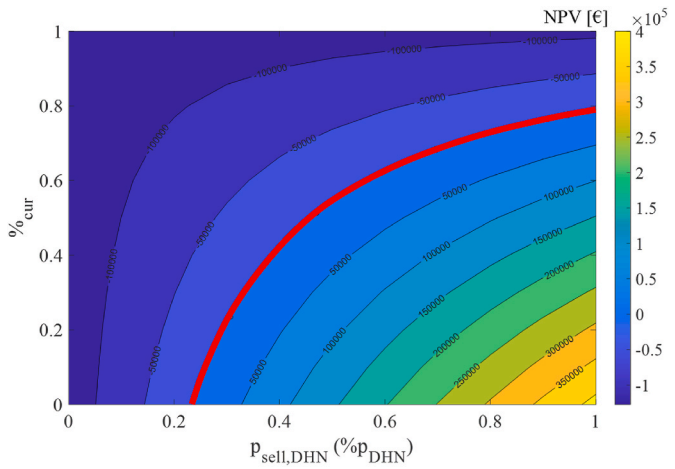

Fig. 14. NPV behavior map for Palermo - 231 m2 - no absorption scenario. NPV: Net Present Value - %cur: Curtailment Ratio – $p_{sell,DHN}$: price of heat sold to the grid expressed as ration of price purchased by the grid.

Table 22
Values of intercept between the zero - NPV front and axes. No sorption scenarios. %cur: Curtailment Ratio – $p_{sell,DHN}$: price of heat sold to the grid expressed as ration of price purchased by the grid.

	Palermo 231 m^2 No-Absorption	Verona 514 m^2 No-Absorption
psell_DHN (NPV = 0)	0.2357	0.2880
$\%_{cur}$ (NPV = 0)	0.7905	0.7365

exercised when extrapolating these results to larger-scale systems, as scalability may introduce new variables and complexities.

- The analysis is conducted assuming two locations with no predominant heating demand (as seen in Northern Europe). Therefore, the key findings should be limited to countries in Southern Europe with similar climatic conditions, with ad hoc studies to be necessarily conducted for other regions.
- The dynamic simulation proved that the introduction of a thermally driven chiller does not lead to evident economic benefits. This deduction cannot be applied to all heating and cooling systems since it is strictly related to the single case study, but it opens the discussion of the need for an in-depth analysis of each system. The interface of multiple sources and technologies should be accurately evaluated from both technical and economic points of view. The economic results, in this case, showed that the absorption chiller could not be the optimal solution, although a renewable and low-cost source supplies it. This study is limited to the analysis of a specific case, future works should rely on a general analysis aiming to define the feasibility of thermally driven equipment included in prosumers' systems.
- Finally, although the use of solar energy and the share of surplus heat will lead to a reduction in the consumption of fossil fuel with consequent environmental benefits during the operational phase, a more detailed environmental analysis—such as a life cycle assessment—will be necessary to gain comprehensive evaluation of impacts over the system's entire lifespan (e.g., including the construction and disposal of solar collectors) thus achieving a multifaced optimization of these systems.

5. Conclusions

In this work, a techno-economic analysis of a high vacuum solar system integrated into a prosumer-based district heating for two locations in Southern Europe was performed. The results indicated that the integration of high-vacuum solar collectors achieves a solar covering fraction ranging between 73.8 % and 27.4 % of the heating demand in the warm Mediterranean climate of Palermo and between 39 % and 12.9 % in a colder climate such as Verona. The use of absorption chillers allows for meeting a fraction of the cooling demand by solar energy, ranging between 33.6 % and 12.3 % for Palermo and between 43 % and 23.6 % for Verona, highlighting the effectiveness of RES in meeting these energy demands. As expected, the yearly efficiency of the solar system is slightly higher in the location with higher solar irradiation (average values of 53.4 % for Palermo), but promising results are achieved in colder Mediterranean climate locations as in the case of Verona (49.9 %). The solar plant can make the user become a prosumer with surplus production in a variable range, according to the surface design: in Palermo, the share of total solar production delivered to the DHN ranges from 53 % to 30.5 %, while in Verona, it varies between 78.7 % and 50.9 %. As expected, peak production (from the substation to the DHN) occurs in summer and during intermediate seasons when heating demand is low. The economic analysis showed that despite higher electricity costs in some cases, significant heat savings ensure profitability. It was also found that the inclusion of absorption chillers may reduce profitability. In addition, the curtailment in solar energy production, which will be frequent in summer, strongly affects the system's profitability. Then, given the large availability of thermal energy during the summer and in light of the growing demand for cooling, it is necessary to have financing systems in place to facilitate the economic profitability of substations with absorption machines. Future research should explore thermal grid interfaces, innovative control strategies, seasonal thermal storage, and market mechanisms to optimize prosumer-based energy systems. Environmental analysis is crucial to validating system effectiveness in reducing emissions, and supporting policymakers in designing financial incentives for wider adoption. Smart grid technologies and digital platforms can further enhance efficiency and reliability. Collaboration among policymakers, energy providers, and consumers is essential to establish a regulatory framework that supports RES investments and thermal energy communities. Additionally, introducing energy market constraints in future studies could refine the application of bidirectional thermal substations in DHNs. Understanding market limitations will help optimize thermal plant sizing and substation control strategies. Advancing renewable integration and power-to-heat technologies will be key to decarbonizing district heating and cooling networks.

CRediT authorship contribution statement

Giuseppe Edoardo Dino: Writing – review & editing, Writing – original draft, Software, Investigation, Conceptualization. **Pietro Catrini:** Methodology, Formal analysis. **Maurizio La Villetta:** Software, Investigation. **Antonio Piacentino:** Supervision, Resources, Project administration.

Declaration of competing interest

The authors declare that they have no known competing financial interests or personal relationships that could have appeared to influence the work reported in this paper.

Acknowledgments

This study was developed in the framework of the research activities carried out within the PRIN 2020 project: "OPTIMISM - Optimal refurbishment design and management of small energy micro-grids", funded by the Italian Ministry of University and Research (MUR).

Nomenclature

$\dot{m}$	Flow rate
DHN	District Heating Network
HE	Heat Exchanger
UA	Global Heat transfer coefficient
CAPEX	Capital Expenditure Cost
OPEX	Operational Cost
CF	Cash Flow
NPV	Net Present Values
WACC	Weighted Average Cost of Capital
ABS	Absorption chiller
HP	Heat Pump
HT	High temperature (Generator loop in the ABS)
MT	Medium Temperature (Condenser loop in the ABS)
LT	Low Temperature (Evaporator loop in the ABS)
Q_{ev}	Cooling capacity at the evaporator
Q_c	Heating capacity at the condenser
C_g	Heating capacity at the generator
P_{el}	Electric power
KPI	Key Performance Indicator
CF	Cash Flow
CAPEX	Capital Expenditure Costs
OPEX	Operational Expenditure Costs
WACC	Weighted Average Cost of Capital

Subscripts

w	Winter operation mode
s	Summer operation mode
i	Initial
f	Final
abs	Absorption chiller
comp	Compression chiller
load	heating or cooling load requested by the user
s	summer mode (cooling)
w	winter mode (heating)
baseline	Baseline scenario
cur	Curtailment

Appendix A. Supplementary data

Supplementary data to this article can be found online at https://doi.org/10.1016/j.energy.2025.136843.

Data availability

Data will be made available on request.

References

[1] Data - Eurostat [Online]. Available: https://ec.europa.eu/eurostat/web/main/data. [Accessed 1 October 2024].

[2] Energy consumption in households - statistics explained [Online]. Available: https://ec.europa.eu/eurostat/statistics-explained/index.php?title=Energy_consumption_in_households. [Accessed 1 October 2024].

[3] Completion of key 'Fit for 55'' legislation [Online]. Available: https://ec.europa.eu/commission/presscorner/detail/en/IP_23_4754. [Accessed 14 March 2024].

[4] I. - International Energy Agency. Renewables. 2019.

[5] DHC scenarios - rewardheat [Online]. Available: https://www.rewardheat.eu/en/DHC-Scenarios. [Accessed 14 March 2024].

[6] Loulou R, Wright E, Giannakidis G, Noble K. Energy technology systems analysis programme. 2016.

[7] Lund H, Werner S, Wiltshire R, Svendsen S, Thorsen JE, Hvelplund F, Mathiesen BV. 4th generation district heating (4GDH): integrating smart thermal grids into future sustainable energy systems. Energy (Calg) Apr. 2014;68:1–11.

[8] Stănişteanu C. Smart thermal grids – a review. The Scientific Bulletin of Electrical Engineering Faculty Apr. 2017;0(0).

[9] Østergaard PA, Lund H. A renewable energy system in frederikshavn using low-temperature geothermal energy for district heating. Appl Energy Feb. 2011;88(2):479–87.

[10] Liew PY, Walmsley TG, Wan Alwi SR, Abdul Manan Z, Klemeš JJ, Varbanov PS. Integrating district cooling systems in locally integrated energy sectors through total site heat integration. Appl Energy Dec. 2016;184:1350–63.

[11] Modelling of waste heat integration into an existing district heating network operating at different supply temperatures. https://doi.org/10.1016/J.SEGY.2023.100104.

[12] Buffa S, Cozzini M, D'Antoni M, Baratieri M, Fedrizzi R. 5th generation district heating and cooling systems: a review of existing cases in Europe. Renew Sustain Energy Rev Apr. 2019;104:504–22.

[13] Boesten S, Ivens W, Dekker SC, Eijdems H. 5th generation district heating and cooling systems as a solution for renewable urban thermal energy supply. Adv Geosci Sep. 2019;49:129–36.

[14] Zeh R, Ohlsen B, Philipp D, Bertermann D, Kotz T, Jocić NJ, Stockinger V, Rosen MA, Khosravi A, Malekan M, Jose J, Pabon G. Large-scale geothermal collector systems for 5th generation district heating and cooling networks. Sustainability May 2021;13(11):6035. 6035.

[15] Mendes G, Ioakimidis C, Ferrão P. On the planning and analysis of integrated community energy systems: a review and survey of available tools. Renew Sustain Energy Rev 2011;15(9):4836–54. Pergamon.

[16] Revesz A, Jones P, Dunham C, Davies G, Marques C, Matabuena R, Scott J, Maidment G. Developing novel 5th generation district energy networks. Energy (Calg) Jun. 2020;201:117389.

[17] Horstink L, Wittmayer JM, Ng K, Luz GP, Marín-González E, Gährs S, Campos I, Holstenkamp L, Oxenaar S, Brown D. Collective renewable energy prosumers and the promises of the energy union: taking stock. Energies Jan. 2020;13(2):421.

[18] Jodeiri AM, Goldsworthy MJ, Buffa S, Cozzini M. Role of sustainable heat sources in transition towards fourth generation district heating – a review. Renew Sustain Energy Rev Apr. 2022;158:112156.

[19] Vivian J, Jobard X, Ben Hassine I, Hurink J. Smart control of a district heating network with high share of low temperature waste heat. In: Conference: 12th conference on sustainable development of energy, water and environmental systems - SDEWES 2017; 2017.
[20] Pipiciello M, Caldera M, Cozzini M, Ancona MA, Melino F, Di Pietra B. Experimental characterization of a prototype of bidirectional substation for district heating with thermal prosumers. Energy (Calg) 2021;223:120036.
[21] Pipiciello M, Trentin F, Soppelsa A, Menegon D, Fedrizzi R, Ricci M, Di Pietra B, Sdringola P. The bidirectional substation for district heating users: experimental performance assessment with operational profiles of prosumer loads and distributed generation. Energy Build Feb. 2024;305:113872.
[22] Kim MH, Kim DW, Lee DW, Heo J. Experimental analysis of Bi-Directional heat trading operation integrated with heat prosumers in thermal networks. Energies Sep. 2021;14(18):5881.
[23] Licklederer T, Hamacher T, Kramer M, Perić VS. Thermohydraulic model of smart thermal grids with bidirectional power flow between prosumers. Energy (Calg) Sep. 2021;230:120825.
[24] Zinsmeister D, Licklederer T, Adldinger S, Christange F, Tzscheutschler P, Hamacher T, Perićperić VS. A prosumer-based sector-coupled district heating and cooling laboratory architecture. 2023.
[25] Dino GE, Catrini P, Buscemi A, Piacentino A, Palomba V, Frazzica A. Modeling of a bidirectional substation in a district heating network: validation, dynamic analysis, and application to a solar prosumer. Energy (Calg) Dec. 2023;284:128621.
[26] Dino GE, Catrini P, Palomba V, Frazzica A, Piacentino A. Promoting the flexibility of thermal prosumers equipped with heat pumps to support power grid management. Sustainability May 2023;15(9):7494.
[27] Gianaroli F, Ricci M, Sdringola P, Pipiciello M, Menegon D, Melino F. Retrofit design and numerical modeling of bidirectional substations for the empowerment of thermal prosumers in district heating networks. Energy Proceedings 2025;51.
[28] Bogdanovics R, Zemitis J, Zajacs A, Borodinecs A. Small-scale district heating system as heat storage for decentralized solar thermal collectors during non-heating period. Energy (Calg) Jul. 2024;298:131260.
[29] Gross M, Karbasi B, Reiners T, Altieri L, Wagner HJ, Bertsch V. Implementing prosumers into heating networks. Energy (Calg) Sep. 2021;230:120844.
[30] Testasecca T, Catrini P, Beccali M, Piacentino A. Dynamic simulation of a 4th generation district heating network with the presence of prosumers. Energy Convers Manag X Oct. 2023;20:100480.
[31] Kauko H, Kvalsvik KH, Rohde D, Nord N, Utne Å. Dynamic modeling of local district heating grids with prosumers: a case study for Norway. Energy (Calg) May 2018;151:261–71.
[32] Li H, Hou J, Hong T, Nord N. Distinguish between the economic optimal and lowest distribution temperatures for heat-prosumer-based district heating systems with short-term thermal energy storage. Energy (Calg) Jun. 2022;248.
[33] Li H, Hou J, Tian Z, Hong T, Nord N, Rohde D. Optimize heat prosumers' economic performance under current heating price models by using water tank thermal energy storage. Energy (Calg) Jan. 2022;239:122103.
[34] Faria AS, Soares T, Cunha JM, Mourão Z. Mutual-benefit of district heating market and network operation for prosumers integration. Energy Sources B Energy Econ Plann Dec. 2023;18(1).
[35] Li H, Sun Q, Zhang Q, Wallin F. A review of the pricing mechanisms for district heating systems. Renew Sustain Energy Rev Feb. 2015;42:56–65.
[36] Youn YJ, Im YH. Analysis of operating characteristics of interconnected operation of thermal grids with bidirectional heat trade. Appl Therm Eng Jul. 2023;229:120608.
[37] Selvakkumaran S, Eriksson L, Svensson I-L. How do business models for prosumers in the district energy sector capture flexibility? Energy Rep 2021;7:203–12.
[38] Qin Q, Gosselin L. Community-based transactive energy market concept for 5th generation district heating and cooling through distributed optimization. Appl Energy Oct. 2024;371:123666.
[39] Tschopp D, Ohnewein P, Stelzer R, Feierl L, Hamilton-Jones M, Moser M, Holter C. One year of high-precision operational data including measurement uncertainties from a large-scale solar thermal collector array with flat plate collectors, located in graz, Austria. Data Brief Jun. 2023;48:109224.
[40] Renewable Energy Agency I. Renewable energy in district heating and cooling: a sector roadmap for REmap; case studies. 2017.
[41] IEA SHC || task 68 || efficient solar district heating systems [Online]. Available: https://task68.iea-shc.org/. [Accessed 10 March 2025].
[42] Huang P, Copertaro B, Zhang X, Shen J, Löfgren I, Rönnelid M, Fahlen J, Andersson D, Svanfeldt M. A review of data centers as prosumers in district energy systems: renewable energy integration and waste heat reuse for district heating. Appl Energy Jan. 2020;258:114109.
[43] Wang D, Carmeliet J, Orehounig K. Design and assessment of district heating systems with solar thermal prosumers and thermal storage. Energies Feb. 2021;14(4):1184.
[44] Palomba V, Dino GE, Frazzica A. Solar-assisted heat pumps and chillers. In: Handbook of climate change mitigation and adaptation. New York, NY: Springer New York; 2021. p. 1–54.
[45] Chèze D, Cuneo A, Macciò C, Porta M, Dino G, Frazzica A, Gabaldón A. Four innovative solar coupled heat pump solutions for building heating and cooling. 2020.
[46] Urbaniak R, Ciupek B, Grobelny P. Experimental analysis of vacuum solar collectors as an auxiliary heating source for residential buildings. Energies Feb. 2025;18(5):1093.
[47] Ancona MA, Branchini L, De Pascale A, Melino F. Smart district heating: distributed generation systems' effects on the network. Energy Proc Aug. 2015;75:1208–13.
[48] Univ. of W.-M. Solar Energy Laboratory. Trnsys simulation environment, vol. 3. Solar Energy Laboratory, Univ. of Wisconsin-Madison; 2018. p. 7–36.
[49] Winterton RHS. Where did the dittus and boelter equation come from? Int J Heat Mass Tran Feb. 1998;41(4–5):809–10.
[50] Bava F, Furbo S. Development and validation of a detailed TRNSYS-matlab model for large solar collector fields for district heating applications. Energy (Calg) Sep. 2017;135:698–708.
[51] Ashrae. "ANSI/ASHRAE/IES Addenda be, bm, bn, bo, bp, br, bs, bu, bv, cf, cl, cm, cq, ct, cu, cv, cw, cy,". 2021.
[52] "Commercial Reference Buildings | Department of Energy." [Online]. Available: https://www.energy.gov/eere/buildings/commercial-reference-buildings. [Accessed: 12-March-2024].
[53] UNI/TR 11552:2014 - UNI Ente Italiano di Normazione." [Online]. Available: https://store.uni.com/en/uni-tr-11552-2014. [Accessed: 12-March-2024].
[54] Kottek M, Grieser J, Beck C, Rudolf B, Rubel F. World map of the köppen-geiger climate classification updated. Meteorol Z Feb. 2006;15(3):259–63.
[55] M. Database, "Meteonorm version 8 - Meteonorm (en)." [Online]. Available: https://meteonorm.com/en/meteonorm-version-8. [Accessed: 4-March-2021].
[56] "Gazzetta Ufficiale." [Online]. Available: https://www.gazzettaufficiale.it/eli/id/1993/10/14/093G0451/sg. [Accessed: 12-March-2024].
[57] "Gazzetta Ufficiale." [Online]. Available: https://www.gazzettaufficiale.it/eli/id/2022/10/17/22A05867/sg. [Accessed: 12-March-2024].
[58] González-Torres M, Pérez-Lombard L, Coronel JF, Maestre IR, Yan D. A review on buildings energy information: trends, end-uses, fuels and drivers. Energy Rep Nov. 2022;8:626–37.
[59] Brand S. "TVP Solar - solar Keymark Certificate,". Jun. 2017.
[60] J. Eric and B. Vad, 'Progression of District Heating-1st to 4th generation.'.
[61] Kältemaschinen [Online]. Available: https://www.baelz.de/systeme/absorptionskaelte. [Accessed 14 March 2024].
[62] Cervera-Vázquez J, Montagud-Montalvá C, Corberán JM. "Science and Technology for the Built Environment Sizing of the buffer tank in chilled water distribution A/C systems,". 2016.
[63] Kuboth S, Heberle F, Weith T, Welzl M, König-Haagen A, Brüggemann D. Experimental short-term investigation of model predictive heat pump control in residential buildings. Energy Build Dec. 2019;204:109444.
[64] "Home - aermec." [Online]. Available: https://global.aermec.com/it/. [Accessed 14 March 2024].
[65] Hiris DP, Pop OG, Balan MC. Preliminary sizing of solar district heating systems with seasonal water thermal storage. Heliyon Feb. 2022;8(2):e08932.
[66] "Technology Data for Individual Heating Plants | The Danish Energy Agency." [Online]. Available: https://ens.dk/en/our-services/technology-catalogues/technology-data-individual-heating-plants. [Accessed: 23-May-2024].
[67] Press E, Badr A, Benmarraze S, Blanco H, Boshell F, Chen Y, Gherboudj I, Jinks B, Nababa M, Parthan B. "Renewable Power Generation Costs in 2020,". 2021.
[68] Papatsounis AG, Botsaris PN, Lymperopoulos KA, Rotas R, Kanellia Z, Iliadis P, Nikolopoulos N. Operation assessment of a hybrid solar-biomass energy system with absorption refrigeration scenarios. Energy Sources, Part A Recovery, Util Environ Eff Mar. 2022;44(1):700–17.
[69] Roncal-Casano JJ, Taddeo P, Rodriguez-Martín J, Muñoz-Antón J, Velasco AA. Techno-economic comparison of a solar absorption chiller and photovoltaic compression chiller. 36th international conference on efficiency, cost, optimization, simulation and environmental impact of energy systems, ECOS 2023. 2023. p. 2661–72.
[70] U. States Department of Energy. "Combined Heat and Power Technology Fact Sheet Series ADVANCED MANUFACTURING OFFICE,". 2017.
[71] "Energy Storage Technology Descriptions-EASE-European Associaton for Storage of Energy Thermal hoT WaTer STorage Thermal energy STorage 1. Technical description.".
[72] SunHorizon." [Online]. Available: https://sunhorizon-project.eu/. [Accessed: 5-June-2024].
[73] "Technology Data for Generation of Electricity and District Heating | The Danish Energy Agency." [Online]. Available: https://ens.dk/en/our-services/technology-catalogues/technology-data-generation-electricity-and-district-heating. [Accessed: 30-May-2024].
[74] Harris D, Figurelli AL. "The WACC for Heating Companies and Heat Exchangers in the Netherlands The WACC for Heating Companies and Heat Exchangers in the Netherlands PREPARED BY PREPARED FOR NOTICE The WACC for Heating Companies and Heat Exchangers in the Netherlands,". 2022.
[75] Electricity price statistics - statistics explained." [Online]. Available: https://ec.europa.eu/eurostat/statistics-explained/index.php?title=Electricity_price_statistics#Electricity_prices_for_non-household_consumers. [Accessed: 5-June-2024].
[76] Prezzi finali dell'energia elettrica per i consumatori industriali - ue a area euro - arera." [Online]. Available: https://www.arera.it/dati-e-statistiche/dettaglio/prezzi-finali-dellenergia-elettrica-per-i-consumatori-industriali-ue-a-area-euro. [Accessed: 5-June-2024].
[77] "La tariffa base del teleriscaldamento e acqua calda sanitaria-Comune di Verona.".